Flameless combustion

in a 2x100kW$_{th}$ furnace: A comparison of experiments with CFD-type simulations

Sjoerd Keizer

Flameless combustion in a 2x100kW$_{th}$ furnace: A comparison of experiments with CFD-type simulations Sjoerd Keizer

Flameless combustion in a 2x100kW_{th} furnace:

A comparison of experiments with CFD-type simulations

Flameless combustion in a 2x100kW_{th} furnace:
A comparison of experiments with CFD-type simulations

MASTER OF SCIENCE THESIS

For the degree of Master of Science in Sustainable Energy Technology at Delft University of Technology

Sjoerd Hendrik Keizer

April 23, 2014

Faculty of Mechanical, Maritime and Materials Engineering (3mE) ·
Department of Process & Energy · Delft University of Technology

This thesis has been approved by the supervisors:

Prof. dr. D.J.E.M. Roekaerts
Dr. ir. W. de Jong

Graduation committee:

Prof. dr. D.J.E.M. Roekaerts	Department of Process and Energy
Dr. ir. R. Pecnik	Department of Process and Energy
Dr. Arvind G. Rao	Faculty of Aerospace Engineering
J. Lu, MSc	Department of Process and Energy

TU Delft

Student Number: 1320491

Contact: mail@shkeizer.com

Cover design: S. H. Keizer

An electronic version of this thesis is available at: http://repository.tudelft.nl/

Printed in the Netherlands

"A theory is something nobody believes, except the person who made it. An experiment is something everybody believes, except the person who made it."

Albert Einstein

Abstract

Flameless combustion is a proven technique for increasing the energy efficiency of hydrocarbon fueled furnaces while also reducing pollutants from being emitted. The increased industrial use of this technology has led to a demand for more information about the possible application for a wider range of appliances. The Delft University of Technology acquired an experimental multi-burner furnace for further research on flameless combustion to do so, in 2007.
Prior research focussed on the effect of several parameters (e.g. cycle time, burner configuration and firing mode) on the performance of the furnace. Further investigation into the formation of a near burner zone gave rise to the construction of a new measurement probe, in order to investigate the species concentrations inside the furnace.
Experiments have been conducted with the new measurement probe for a range of different furnace settings. Profiles have been made from the collected data, to show the species concentration along a line in the furnace perpendicular to the wall and along the symmetry axis of the burner.
Three cases of CFD simulations have been compared with the experimental results, with moderate success due to differences between the setup and the CFD model.
An introduction into the field of Design of Experiments was made. The technique is suggested to be used for improvement of the design generation for the experimental campaigns. This should be done using dedicated software programs.
Lastly, several adaptations have been suggested to be made for the furnace and peripheral equipment e.g. installation of a static mixer for biogas fuel experiments and a new gas analyzer for increasing measurement accuracy.

Keywords: Flameless combustion, multi-burner, flameless oxidation, species probe, energy efficiency.

Contents

1 Introduction **3**
- 1.1 Background . . . 4
- 1.2 Flameless combustion . . . 5
- 1.3 Thesis outline . . . 10
- References . . . 10

2 Design of Experiments **13**
- 2.1 Introduction . . . 14
- 2.2 Historical overview . . . 14
- 2.3 Design of Experiments . . . 16
- 2.4 MEEC experimental design guide . . . 19
- References . . . 19

3 MEEC Furnace **21**
- 3.1 Furnace Design . . . 22
- 3.2 Peripheral equipment . . . 24
- 3.3 Species Probe . . . 28
- 3.4 Furnace adaptations . . . 30
- 3.5 Encountered problems . . . 32
- References . . . 34

4 Experiments **37**
- 4.1 Experimental campaign . . . 38
- 4.2 Firing mode . . . 39
- 4.3 Flow patterns . . . 40
- 4.4 Species Probe . . . 41
- References . . . 42

5 Computational Fluid Dynamics **43**
- 5.1 MEEC furnace: three cases . . . 44
- References . . . 45

6 Results & Discussion **47**
6.1 Introduction 48
6.2 Cooling air - Parallel 48
6.3 Cooling air - Staggered 1 52
6.4 Burner air - Parallel 56
6.5 Regenerative flue gas comparison 59
6.6 CFD 59
6.7 Species probe - Boudouard occurrence 62
References 63

7 Conclusions & Recommendations **65**
7.1 Conclusions 66
7.2 Recommendations 67

A Data analysis **69**

B Heat up with Flame to Flox routine **75**

C Near burner zone **77**

D Species Probe heat extraction **79**

Nomenclature

Symbol	Units	Description
C_j	[$\mathrm{m}^3/\mathrm{s}\sqrt{Pa}$]	Calibrated conversion constant for plate j
CTE	[%]	Cooling tube efficiency
c_p	[kJ/kg K]	Specific Heat
K	[−]	Karlovitz stretch factor
N_i	[−]	Number of components in i
n_i	[mol]	Amount of species i in the flue gas
M_i	[kg/mol]	Molar mass of component i
p	[Pa]	Pressure
p°	[101325Pa]	Reference pressure
$Q_{fuel,in}$	[kW]	Heat generated from combustion
R	[8.314J/mol K]	Universal gas constant
$\bar{T}$	[K]	Mean temperature
T°	[273.15K]	Reference temperature
T_i	[K]	Temperature on position i
T_u	[−]	Temperature uniformity
u'	[−]	Root mean square turbulent velocity
u_l	[m/s]	Unstretched laminar burning velocity
$X'X$	[−]	Information matrix
$\left\|(X'X)^{-1}\right\|$	[−]	Determinant of the information matrix $X'X$
x_i	[−]	Molar fraction of component i
Greek		
ΔH	[J/kg]	Heating value
δ_l	[m]	Laminar flame thickness, ν/u_l
γ	[−]	Stoichiometric required air
λ	[m]	Taylor length scale of turbulence
λ	[−]	Excess air ratio
ρ	[kg/m^3]	Density
$\Phi_{m,i}$	[kg/s]	Mass flow of component i

$\Phi_{m,flue}^{regen}$	[kg/s]	Mass flow of flue gas over the regenerator
$\Phi_{v,i}^{\circ}$	[m^3/s]	Volume flow of component i at normal conditions
ξ_j	[−]	Number of atoms in species j
subscripts		
air		Air
C		Carbon
$cool$		Cooling tube
$flue$		Flue gas
$fuel$		Fuel
H		Hydrogen
i		i-th component
j		j-th component
$regen$		Regenerator
$stack$		Stack

Chapter 1

Introduction

This chapter will introduce the reader into the research area of flameless combustion, after which the research objectives will be discussed.

1.1 Background

Since the beginning of the Industrial Revolution an increase of energy consumption worldwide has been recorded together with an increase of the Greenhouse effect [1]. This effect is caused by extraction and consumption of hydrocarbons from the Earth. These hydrocarbons can form, by chemical conversion (such as combustion type of) reactions, a host of different types of gases such as CO_2, CH_4 and N_2O which all have their own Global Warming Potential (GWP). This GWP is an index used to compare the relative radiative forcing of different gases without directly calculating the changes in atmospheric concentrations. The GWP is also a function of the atmospheric lifetime of the gas among other things [2].
In recent years, global awareness has increased of the fact that the emission of these pollutants into the atmosphere might be related to the global temperature increase on Earth. In order to reverse the observed trend of global warming or to prevent it all together new research fields have appeared since the oil crisis in the late eighties of the last century. One of these new fields focusses on increasing the efficiency of combustion processes by creating new designs and techniques, mostly creating a good mixture of fuel and air and using a high rate of gas recirculation with temperatures above the autoignition temperature of the fuel. The autoignition temperature is the minimal temperature required to initiate combustion and depends on the kind of fuel as well as the oxygen concentration of the diluted air. High recirculation ratios can be achieved by internal flows originating from high momentum jets or by external flows recirculating the hot exhaust gases from operating furnaces. Exhaust recirculation can be an effective method to reduce the flame temperature and smoothen the temperature distribution inside a furnace. Due to high recirculation ratios and lower temperatures, a different type of flame can be observed and thus a different type of reaction zone appears (Appendix C). During the discovery period of this process several names were given by research groups across the world, resulting in a range of names for the same process. One of the first publications was by Wünning and Wünning [3] from WS Wärmeprozesstechnik GmbH and they proposed Flameless Oxidation (FLOX) as a name for the process, which is somewhat unfortunate because there are also different types of oxidation reactions (think of rust formation due to iron oxidation) besides combustion. Not much later a Japanese research group [4] proposed HiTAC (high temperature air combustion) as a more appropriate name. However, this too is not convenient due to the term "high temperature" because it is not a requirement for the process. Moreover, there is no fixed definition for when a certain temperature is "high", "moderate" or "low". This classification problem brings us to another research group, Cavaliere et al. [5], which uses the term

MILD combustion "moderate and intense low oxygen dilution". The problem with this definition is that it is rather complex.
The term which will be used in this thesis is Flameless Combustion as it is the most appropriate name describing the process while at the same time preventing ambiguity.

1.2 Flameless combustion

Theory Flameless combustion was found to be a promising technique for increasing the energy efficiency of hydrocarbon fueled furnaces while also reducing pollutants from being emitted. The principle of flameless combustion will be briefly explained here.
Instead of injection of fuels and air with low momentum, flameless combustion can be achieved by injecting fuel and air jets with high momentum directly into a hot confined space with temperatures above the autoignition point of the fuel. The high momentum of the jets causes the hot flue gases to be entrained. The jets mix with the fuel inside of the furnace (Appendix C) while achieving much higher recirculation rates then would be possible for conventional flames to be stable. The overall burning rate in flames will hereby increase due to the added turbulence in the flow field [6]. A way of indicating the amount of introduced turbulence in the flow field is by the strain rate of the flame. This can be expressed as the Karlovitz stretch factor K [7], see Equation 1.1.

$$K = (u'/\lambda)\,(\delta_l/u_l) \tag{1.1}$$

Here, u' is the root mean square (rms) turbulent velocity which increases the turbulent burning. When u' is divided by the Taylor scale of turbulence λ for isotropic turbulence, it defines the rms strain rate. The flame can be extinguished if this rate becomes sufficiently high. The Karlovitz stretch factor is defined after normalization by the chemical time δ_l/u_l.
The high momentum injection of the jets causes the reaction zone to be stretched out and subsequently the flame to be extinguished (under standard conditions). However, due to the temperatures in the furnace being higher than the autoignition point, the mixture will spontaneously ignite and burn in a wide range of conditions. The resulting area and volume of the reaction zone will be substantially larger, compared to the reaction zone of conventional flames, which can be characterised by their flame front. Due to this increase of the reaction zone, more mass has to be heated by the same amount of heat from the combustion reaction, hereby resulting in a lower temperature peak and a more uniform temperature

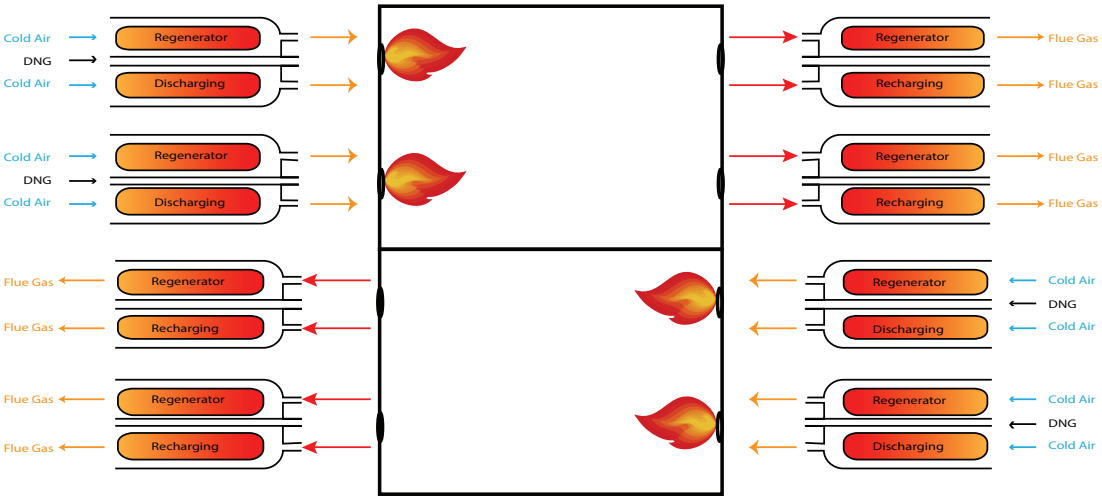

Figure 1.1: Alternating operating mode of the MEEC regenerative combustion furnace with temperature gradients displayed over the ceramic honeycomb heat exchangers.

distribution in the confined space.
The second important aspect for flameless combustion is the regeneration of heat from the hot exhaust gases. During the regenerating phase of the burner, the hot flue gases flow over a ceramic honey comb heat exchanger, located within the burner. In turn, the heat exchanger heats up and can again transfer the stored energy back to the combustion air in the next active cycle, where the flow is reversed. As such, the furnace has to be equipped with at least two burners so they can regenerate in an alternating fashion, see Figure 1.1. For a complete overview of the operating ranges for flameless combustion see Figure 1.2.

Reaction fundamentals A better understanding of the phenomena of flameless combustion can be attained when special attention is given to the formation of emissions inside and outside of the reaction zone. The decrease in furnace temperature during flameless operation has a direct effect on the formation of CO_2, CO and NO_x. CO-emissions are negative outcomes of incomplete combustion due to sub-stoichiometric oxygen presence in the (local) reaction zone. Stoichiometric combustion is the ideal combustion process where the fuel is burned completely. In the case of stoichiometric ($a = 2, b = 0$) methane (CH_4) combustion with atmospheric air this would be as shown in Equation 1.2. A more practical approach is to have an excess amount of air by increasing the air supply ($a > 2$) to ensure the flue gases contain some excess oxygen ($b > 0$) and no CO.

$$CH_4 + a\,(O_2 + 3.76N_2) \rightarrow CO_2 + 2H_2O + \mathrm{b}O_2 + 3.76aN_2 \tag{1.2}$$

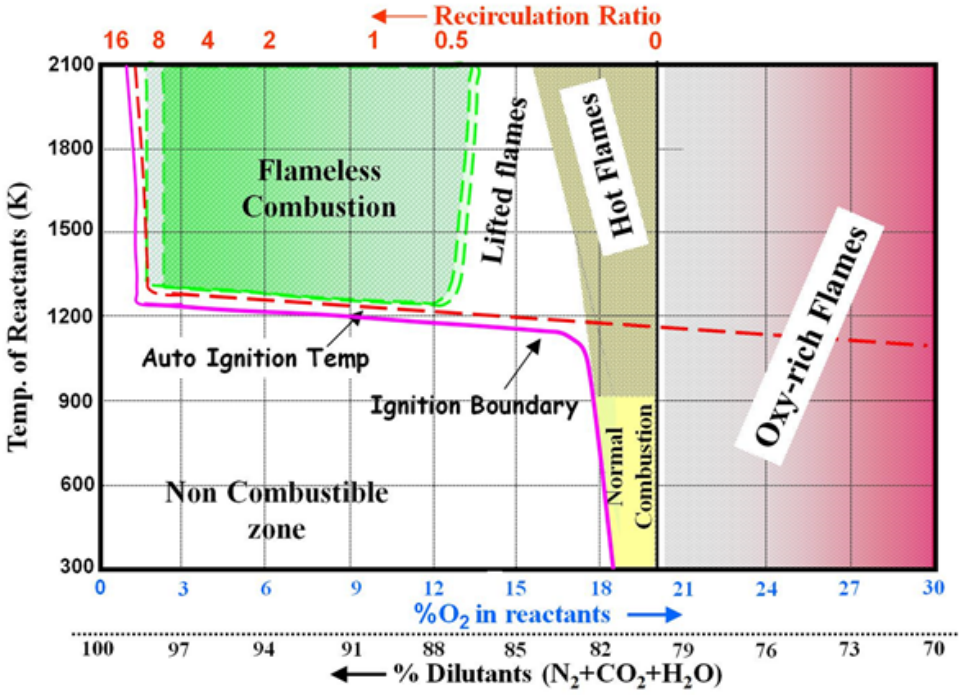

Figure 1.2: Diagram showing the operating regimes for flameless combustion [8].

To gain insight into the formation of the products of incomplete combustion we have to look into the reaction mechanisms for the specific species.
NB: From prior operation of combustion furnaces it is known that when temperatures of the furnace drop and become lower than $\approx 950°C$ the reaction kinetics of CO formation become dominant compared to the formation of nitric oxides. This is important to take into account during the control of the furnace and during analysis of the data.

Carbon mono- and dioxide reaction mechanism The reaction mechanism for carbon monoxide and carbon dioxide from the combustion of hydrocarbons can be described by a two-step process with CO formation as the first step and CO_2 formation following as the second step [9], see Equations 1.3.

$$\begin{aligned} CO + \mathrm{O}_2 &\rightleftharpoons CO_2 + O \\ O + H_2O &\rightleftharpoons O_2 + OH \\ CO + OH &\rightleftharpoons CO_2 + H \\ H + O_2 &\rightleftharpoons OH + O \end{aligned} \tag{1.3}$$

Equations 1.3 show two intermediate steps for the reaction from CO to CO_2 which involve OH as intermediate species. The rate at which CO is consumed is much higher in the step with the OH radical, resulting in the first step being the rate determining step for the consumption of CO.
Noteworthy is the presence of the OH radical because it can only be present whenever and wherever there is a combustion process ongoing. This knowledge is often used to visualize combustion processes with OH laser-induced predissociative fluorescence (OH-LIPF) [10] techniques. These visualisations can then be used to validate Computational Fluid Designs (CFD) also.

Nitric oxides reaction mechanism There are four pathways for the formation of nitric oxides that involve nitrogen from the supplied air in the temperature operating range of the furnace at the Delft University of Technology: the thermal NO, the prompt NO, the N_2O intermediate and the reburning. These will be discussed because of their relevance in Chapter 5.

- *Thermal - (Zel'dovich)*
  The residence time of nitrogen molecules in the presence of high temperatures determine the formation of NO_x along this pathway. To be able to apply this mechanism and follow the pathway, it is often simplified as steady-state approximation and consists of three reactions, first described by Zel'dovich [11] and later extended with the hydroxyl radical reaction by G. A. Lavoie et al. [12]. The physical principle of these steps can be best understood as follows. There is an initial rapid buildup in concentration of radicals from step 1, but these are destroyed in the second step by a faster rate resulting in the overall reaction as displayed. In this case, the first step is rate limiting due to the extremely high reaction rate of the second step [13]. The reaction steps can be seen in Equations 1.4.

$$\begin{aligned} N_2 + O &\rightleftharpoons NO + N \\ N + O_2 &\rightleftharpoons NO + O \\ N + OH &\rightleftharpoons NO + H \end{aligned} \tag{1.4}$$

  It has to be noted that this thermal pathway becomes the dominate path when temperatures are higher than $\approx 1800K$, which explains the benefits of reducing the peak temperature beneath this temperature in flameless combustion furnaces.

- *Prompt - (Fenimore)*
  The prompt pathway of nitric oxide formation is linked to the combustion of hydrocarbons and depends on local combustion conditions instead of the

temperature. It thanks its name to the quick (prompt) formation of NO before the thermal pathway can be of importance. The general scheme is that hydrocarbon radicals react with molecular nitrogen and form amines and cyano compounds that form intermediate species. These then react in the next step to eventually form NO. The primary reaction step is shown in the first equation of Equations 1.5. This is determined by the reaction rate of the steps, resulting in the slowest step being the rate limiting one.

$$\begin{aligned} CH + N_2 &\rightleftharpoons HCN + N \\ C + N_2 &\rightleftharpoons CN + N \end{aligned} \tag{1.5}$$

This is not the complete reaction, however, for equivalence ratios of less than 1.2. If this were the case, the first step of the equation should be written as in Equations 1.6 [14]:

$$\begin{aligned} HCN + O &\rightleftharpoons NCO + H \\ NCO + H &\rightleftharpoons NH + CO \\ NH + H &\rightleftharpoons N + H_2 \\ N + OH &\rightleftharpoons NO + H \end{aligned} \tag{1.6}$$

- *N_2O intermediate*
  The intermediate pathway plays an important role in the combustion with lean combustion mixtures in low temperatures [15]. This makes it especially important for the appliance of flameless combustion. The reaction steps that are involved in this mechanism, are displayed in Equations 1.7.

$$\begin{aligned} N_2 + O + M &\rightleftharpoons N_2O + M \\ N_2O + H &\rightleftharpoons NO + NH \\ N_2O + O &\rightleftharpoons NO + NO \end{aligned} \tag{1.7}$$

- *NO_x reburn*
  The instantaneous NOx reburning mechanism is a pathway whereby NO reacts with hydrocarbons and is subsequently reduced and follows the general formula as shown in Equation 1.8.

$$CH_i + NO \rightarrow HCN + products \tag{1.8}$$

  High temperatures ($1600 < T < 2100$) require the use of the following three reactions [9]:

$$\begin{aligned} \mathrm{CH + NO} &\xrightarrow{k_1} \mathrm{HCN + O} \\ \mathrm{CH_2 + NO} &\xrightarrow{k_2} \mathrm{HCN + OH} \\ \mathrm{CH_3 + NO} &\xrightarrow{k_3} \mathrm{HCN + H_2O} \end{aligned} \tag{1.9}$$

1.3 Thesis outline

New developments After several experimentally based studies, performed on the Multi-excess enthalpy combustion (MEEC) furnace at the Delft University of Technology, in an effort to gain better insight into the field of flameless combustion, several research extension possibilities were recommended [16]. One of these recommendations encompassed the wish of gaining more information on species concentration in the furnace. An in situ measurement probe was constructed in order to directly extract flue gases from the furnace for analysis, to achieve this objective.

Research Questions The goal of this thesis is to verify if such type of experiments can successfully be executed and if so, to what extend the prior knowledge of the near burner zone, among other zones, agrees with the obtained experimental and computational results.
A second goal is to identify whether or not a Design of Experiments framework can be used as an alternative, more efficient, way of setting up the experimental campaigns.

Research Methodology The MEEC furnace will be used, in a varying selection of firing modes, for which the species probe shall be inserted into the furnace at predefined depths. The results will be presented and compared to computational results.
A literature study will be performed into the field of Design of Experiments for similar experimental setups. After which a recommendation will be given if this approach is desirable or not.

References

1. EnerData. Global energy statistical yearbook. `http://yearbook.enerdata.net` (2014). [Online; accessed 27/03/2014].
2. Administration, U. E. I. Glossary. `http://www.eia.gov/tools/glossary/index.cfm?id=G` (2014).
3. Wünning, J. A. & Wünning, J. G. Flameless oxidation to reduce thermal no-formation. *Progress in Energy and Combustion Science* **23**, 81–94 (1997).
4. Katsuki, M. & Hasegawa, T. The science and technology of combustion in highly preheated air. *Symposium (International) on Combustion* **27**, 3135–3146 (1998).
5. Cavaliere, A. & de Joannon, M. Mild combustion. *Progress in Energy and Combustion Science* **30**, 329–366 (2004).

6. Bradley, D. *Chapter 2 - Fundamentals of Lean Combustion*, 19–II (Academic Press, Burlington, 2008).
7. Bradley, D., Lau, A. K. C. & Lawes, M. Flame stretch rate as a determinant of turbulent burning velocity. *Phil. Trans. R. Soc* 357387 (1992).
8. Rao, G. A. & Levy, Y. A new combustion methodology for low emission gas turbine engines. In 8^{th} *HiTACG conference* (2010). Poznan.
9. FLUENT, A. Fluent 6.3 user's guide (2006).
10. Plessing, T., Peters, N. & Wünning, J. G. Laseroptical investigation of highly preheated combustion with strong exhaust gas recirculation. *Symposium (International) on Combustion* **27**, 3197–3204 (1998).
11. Zel'dovich, Y. B. The oxidation of nitrogen in combustion to reduce thermal no-formation. *Acta Physiochimica U.S.S.R.* **21**, 4 (1946).
12. Lavoi, G. A., Heywood, J. B. & Keck, J. C. Experimental and theoretical study of nitric oxide formation in internal combustion engines. *Combustion Science and Technology* **1**, 313–326 (1970).
13. Turns, S. R. *An Introduction to Combustion: Concepts and Applications* (2012), third edn.
14. Miller, J. A. & Bowman, C. T. Mechanism and modeling of nitrogen chemistry in combustion. *Progress in Energy and Combustion Science* 287–338 (1989).
15. Dagaut, P., Glarborg, P. & Alzueta, M. U. The oxidation of hydrogen cyanide and related chemistry. *Progress in Energy and Combustion Science* 1–46 (2008).
16. Danon, B. *Furnaces with multiple flameless combustion burners.* Ph.D. thesis, Delft University of Technology (2011).

Chapter 2

Design of Experiments

2.1 Introduction

Experiments have always been present over the course of human history. Whether it was because of a theory had to be tested, simply because it was possible or maybe just for fun, they all had different approaches and were of different types. Nowadays, time and money are becoming more important resulting in the need for shorter and more efficient experimental campaigns. At the same time, there is also a need for more complex experiments that can take into account multiple factors and response, see Figure 2.3, at the same time while simplifying the analysis routine.
The immense amount of information that can be gained from using analytical methods such as Design of Experiments for setting up experimental campaigns resulted in this Chapter being made. Design of Experiments is a framework that contains methodologies and techniques that help the researcher to conduct better experiments and analyze experimental data more efficiently [1]. This chapter will give a short introduction into the field of statistical methodologies and technologies in continuous (furnace) processes with the goal of creating a guideline for future research to save costly time and gain a better insight generating computer assisted designs (with programs such as JMP, MiniTab, DesignExpert [2, 3, 4]). Due to a restriction in time it was chosen not to conduct an actual statistical analysis of obtained data from experiments. Instead an overview will be given of the history of the experimental design analysis with subsequently a brief overview of statistical methods that show great potential for application on the MEEC furnace experimental setup.

2.2 Historical overview

The first type of experiments were done as one-factor-at-a-time (OFAT) [5] and this methodology is still used by many scientists [6]. The main argument against using this technique is the amount of experiments that have to be done in order to reach to a firm conclusions. Sofar, this has also been the case for the research on the MEEC furnace.
Statistical experimental design has seen a couple of development periods in recent history. The first period was in the 1920s and 1930s in which the OFAT approach was questioned for its efficiency and time-consuming nature by R.A. Fisher. Fisher focussed on agricultural and biological problems by suggesting Design of Experiments (DoE) to be performed [7]. In order to do this he developed several analytical frameworks and methodologies which could be used for scientific research. The most important contributions that were made by Fisher

encompass the requirements for any statistical experiment to have the following three features: randomization, replication and blocking. For further information about these terms, readers are referred to Montgomery [5]. Ultimately, Fisher became most famous for his analysis of variance (ANOVA) [5] method as a statistical test for comparing the means of several groups and check if they are equal, therefor generalizing the t-test [8] to more than two groups and his conceptual formulation of factorial design.

The second period began when the end of World War II was near and ended in the 1970s. It was then that the DoE movement gained more interest from the chemical and process industry which wished to optimize their production processes. The Response Surface Method (RSM) [9] came forth from this movement, with important contributions of G.E.P. Box [10]. Later in this 30 year period the focus shifted towards creating optimal experimental design using computer assisted tools. These tools were able, although very limited at the time, to determine an optimal design based on specific requirements for the experiment that could be set by the experimentalist.

The third period commenced in the late 1970s and 1980s in which developments once again saw a boost by the activities of G. Taguchi [11] that were focussed on robust parameter design. These involve several type of factors such as difficult and easy to change factors (during or in between experiments), which inherently make the design more complex. To solve this problem, he developed fractional factorial design methods and other orthogonal array based techniques.

The fourth and current period features developments regarding the application of the often difficult to understand techniques for the average scientist. Thus, user-friendly statistical design tools were created and are constantly updated to make the learning-curve and entry-difficulty smaller. With the increase of computational power the developed techniques in the second period are becoming more interesting in recent times, resulting in optimal designs that are created for specific experiments. It is this type of computer assisted approach from which the research on the MEEC furnace will benefit most.

The fourth period also covers the arrival of Six Sigma tools that are tailored more towards continuous improvement within companies and relying heavily on statistical frameworks. The Six Sigma approach will not be discussed in this thesis because of the limited applicability in the current experimental setup. If the reader wants to know more about this topic, please refer to Hild et al. [12].

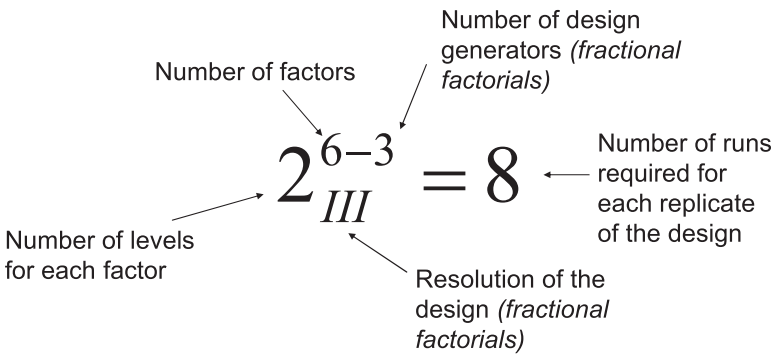

Figure 2.1: An example of a two-level (1/8 fractional) factorial design [13].

2.3 Design of Experiments

One-factor-at-a-time (OFAT) and Factorial designs Most often the OFAT technique is used simply because it is the methodology that seems to come naturally, just like trial-and-error experiments in day-to-day life. The name of the technique is self-explanatory in that one factor will be changed for each individual experiment.
Researchers often want to incorporate a more advanced design so the logical next step usually involves a small literature study into statistical design theory and often leads to the old-fashioned approaches that have been developed in the second period as described in Section 2.2. An example of these techniques are the (full or fractional) factorial designs, also known as 2^k-factorial designs. The core principles are displayed in Figure 2.1 and Figure 2.2. The fundamental principle of the factorial design is that it is desirable to run experiments for all the corner points (Figure 2.2) for the highest possible resolution, if time permits. Also, addition of center and middle points are possible in case the researcher believes non-linear effects are present. However, leaving out corner points results in a loss of resolution and a less optimal design, reducing the efficiency of the process. The total number of points for which data has to be collected can be expressed as seen in Figure 2.1. The approach of taken all of the points results in a dramatically increasing total number of runs required for increasing numbers of factors, levels and for situations where a high resolution design is desirable (more information in Montgomery [5]). Increasing the number of runs is not possible in all occasions due to limitations on the available time and money.

General model A solution to the increasing number of runs required for the factorial designs, is to use a smarter approach which can be described as the general model for Design of Experiments. This general model is visually presented in

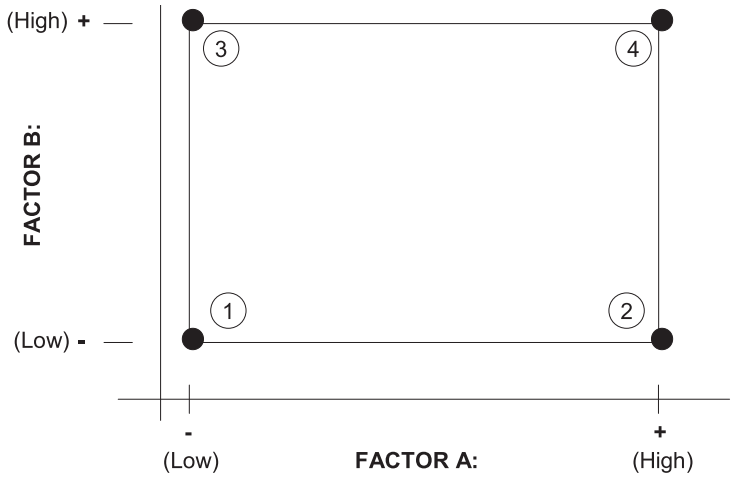

Figure 2.2: An example of the classical type of factorial design is displayed in this figure. The main drawback of these designs are the increasing complexity and required runs for a high number of factors and responses.

Figure 2.3. The model, which is normally used for discrete systems, consists of inputs, outputs and responses. Traditionally these variables have to be determined and defined before conducting the experiments but without proper knowledge of the complexity of the system, it is probable the researcher will encounter problems with correlation and causation from the data. Design of Experiments can help the researcher with effects that seem to be the result of factor X but could in fact be the interaction effect of X and Z to produce the response Y. These interaction effects are undesirable as they make it more difficult to understand what is happening in the process.

Optimal design Section 2.2 mentioned an "optimal" design but did not specify what optimal means in this context. Several types of optimal designs exist (D, I & A) and they differ in the criterion that defines them. For instance the D-optimality criteria seeks to minimize or maximize $\left|(X'X)^{-1}\right|$ which is the determinant of the information matrix $X'X$. While the I-optimality criteria seeks to minimize the average prediction variance over the design space. Ultimately by minimizing the variance there is a maximization of the information.
Most often, and in the case of the MEEC furnace, the *D-optimal* design should be used which is best described with the following definition by Montgomery [5]:

> [...] a design that minimizes the variance of the model regression coefficients is called a *D-optimal* design. The D terminology is used because these designs are found by selecting runs in the design to

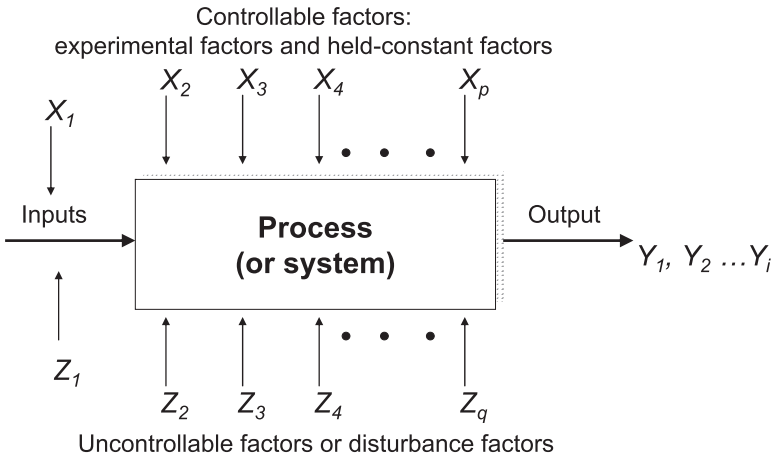

Figure 2.3: In this figure a representation is given for a process under experimentation. Factors that affect the system are divided into controllable (Xs) and uncontrollable (Zs) and result in the responses (Ys) of the system [13].

> maximize the determinant. The 2^k design is a *D-optimal* design for fitting the first-order model or the first-order model with interaction.

So speaking of optimal design a matrix of factors, disturbances and responses can be "optimized" for a given amount of replication, reruns and level of detail. Modern analytical software packages include these tools and can often calculate the required designs in a couple of seconds [14]. After the generation of the experimental campaign design the only thing the researcher has to do is the experiments and analyse the data.

Split-plot designs The MEEC installation takes time to heat up (Appendix B) so it is time-consuming to perform the experiments. This means that the design has to be able to take into account a number of variables combined together with a factor that describes the difficulty of changing it. Furthermore, randomisation and especially replication of the runs in the design can be difficult to fully incorporate. Randomisation of the experimental settings require many manual changes to the furnace and this is often difficult to incorporate without introducing some form of human error in turning the valves etc. Replication is mainly difficult to incorporate because of the long time it takes to obtain a trustworthy data set, see Appendix A & B for additional information about heat up and data gathering.
One method to circumvent the problem of hard-to-change factors is by using a split-plot design approach [15]. Essentially a split-plot design is an experiment that is done in groups of hard-to-change factors, such as burner air flow rate,

while varying the other factors. Splitting the design space in to multiple groups makes it more difficult to analyze to results and adds more importance to the correct design of the whole experiment. Computer assisted design tools can help with predicting the efficiency of the experimental campaign, based on split-plot designs, beforehand and can also present alternate versions of the design. This leaves the decision of which design is preferred completely to the researcher, depending on the nature of the experiment. The split-plot approach originated from agricultural problems that often have hard-to-change factors.
The main benefit of the split-plot design is the relative ease of setting it up when making use of computer assisted design generation. The design tools were not available before 2005 [15], to generate custom made designs for a specific type of experiment, in commercially available statistical software packages. However, now they are available and thus much can be gained with relative ease.

2.4 MEEC experimental design guide

Each experimental campaign for the MEEC furnace should be started with a thorough research into the subject or effect that has to be studied. In order to do so, the following steps could be followed as a design guide to optimize the planning of the campaign:

1. Set the goal of the experiment e.g. maximizing the cooling tube efficiency (Appendix A) or minimizing NO_x formation in the furnace.
2. Determination of the factors, levels and ranges.
3. Determination of the response variables on which the focus will be.
4. Choose the type of design by generating it with a statistical software package.
5. Experimental campaign.
6. Statistical analysis on the raw data using a statistical software package.
7. Draw up conclusions and recommendations.

When following the steps mentioned above an optimisation can be achieved between gathering high qualitative data versus the time that was required to do the experiments.

References

1. Wu, C. F. J. & Hamada, M. *Experiments: planning, analysis, and parameter design optimization* (Wiley, 2000). New York.

2. JMP, S. Statistical discovery software. `http://www.jmp.com/` (2014). [Online; accessed 04/04/2014].
3. Inc, M. Minitab statistical software. `http://www.minitab.com` (2014). [Online; accessed 04/04/2014].
4. Stat-Ease. Design expert. `http://www.statease.com` (2014). [Online; accessed 04/04/2014].
5. Montgomery, D. C. *Design and Analysis of Experiments* (John Wiley & Sons, Incorporated, 2012), 8th edn.
6. Czistrom, V. One-factor-at-a-time versus designed experiments. *The American Statistician* **53(2)**, 126–131 (1999).
7. Fisher, R. A. *The Design of Experiments* (Macmillan Pub Co, 1935).
8. Dekking, F. M., Kraaikamp, C. & Lopuhaå, H. P. *A Modern Introduction to Probability and Statistics: Understanding Why and How.* (Springer, 2005), 1st edn.
9. Myers, R. H., Montgomery, D. C. & Anderson-Cook, C. M. *Response Surface Methodology: Process and Product Optimization Using Designed Experiments* (Wiley, 2009), 3rd edn.
10. Box, G. E. P., Hunter, W. G. & Hunter, J. S. *Statistics for Experimenters* (Wiley, New York, 2005), 2nd edn.
11. Taguchi, G. Systems of experimental design. *Kraus International Publications* **I & II** (1987).
12. Hild, C., Sanders, D. & Cooper, T. Six sigma* on continuous processes: How and why it differs. *Quality Engineering* **13**, 1–9 (2000).
13. Vanhatalo, E. *Contributions to the use of Designed Experiments in Continuous Processes: A Study of Blast Furnace Experiments.* Ph.D. thesis, Luleå University of Technology (2007).
14. Jones, B. & Nachtsheim, C. J. A class of three-level designs for definitive screening in the presence od second-order effects. *Journal of Quality Technology* **43** (2011).
15. Goos, P. & Jones, B. *Optimal Design of Experiments: A Case Study Approach* (Wiley, 2011), 1st edn.

Chapter 3

MEEC Furnace

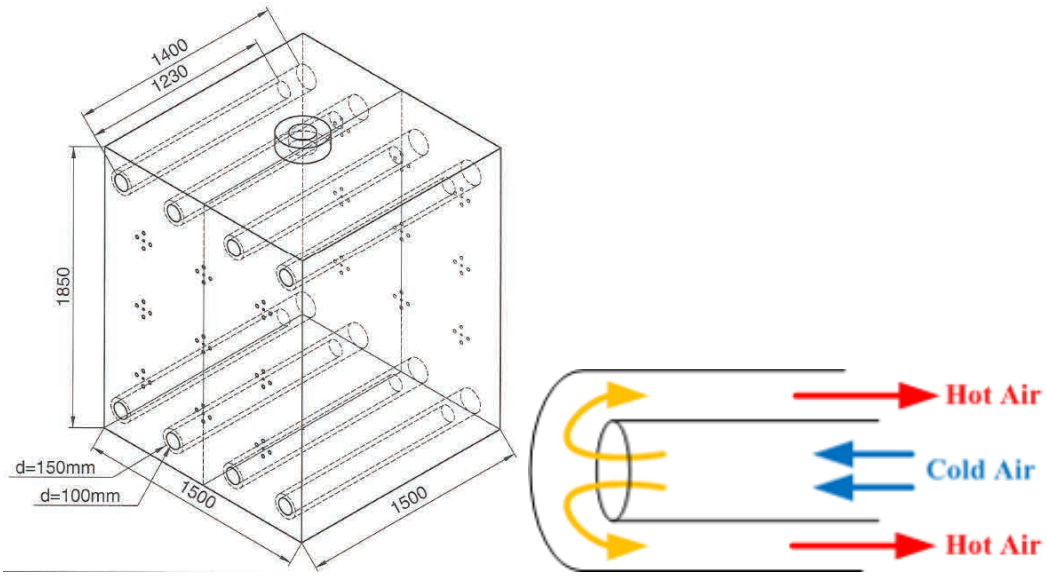

Figure 3.1: On the left a sketch of the MEEC furnace. All dimensions are in mm. On the right the air flows in the cooling tubes are shown schematically.

3.1 Furnace Design

The MEEC (Multi-Excess Enthalpy Combustion) furnace located at the Delft University of Technology is a cube shaped box with inner dimensions of 1500 x 1500 x 1850mm (length x width x height), see Figure 3.1. The walls are insulated by a layer of firebricks and a layer of fibrous insulation blanket for a total thickness of 300mm. Both layers are manufactured by Thermal Ceramics [1, 2]. The heat generation comes from the combustion of fuel and is facilitated by regenerative burners. The burners are of the REGEMAT CD 200 type and were manufactured by Wärmeprozesstechnik GmbH. They have a thermal design capacity of $100kW_{th}$ each with a total combined furnace capacity of $300kW_{th}$ during operation. The conducted experiments during this thesis have used two out of the three burners on each side, resulting in a maximum heating capacity of $200kW_{th} \pm 10kW$. For information regarding the heat up of the furnace see Appendix B.

The regenerative burners, see Figure 3.2, are fitted with ceramic honeycomb heat exchangers for the regeneration of the flue gases. The honeycomb structure maximizes the surface area over which the gases have to flow resulting in a larger amount of heat exchanged. During operation around 80% (see Chapter 6 for measured values) of the flue gases flow over the heat exchanger and 20% leave the furnace through the stack (top of the furnace, see Figure 3.1 or 3.3).

The furnace is equipped with eight cooling tubes to simulate a heat sink and to

Figure 3.2: Different views of the REGEMAT CD 200 type regenerative burners, manufactured by Wärmeprozesstechnik GmbH.

prevent the furnace from damage due to the temperatures becoming too high. These cooling tubes are located at the top and bottom side of the furnace volume for control over the conditions inside to achieve a steady-state operation. Each of the tubes are designed to extract a maximum of $25kW_{th}$ resulting in a total cooling tube capacity of: $\sum = 200kW_{th}$. It has, however, been concluded [3] that this estimate was too optimistic and less is available in practice. The extraction of heat is the result of air cooling through the tubes as seen in Figure 3.1. The cold air is provided by a fan through the inner tube and subsequently flows back out of the tube after hitting the wall at the end of the outer tube. This method was chosen because of the aim to have a small temperature gradient over the cooling tubes outer surface. Air was chosen as preferred medium instead of water in spite of the fact that water has a higher heat capacity ($C_{p,water} > C_{p,air}$) because the danger would be too high (superheated steam will form) in case of cooling tube leakages (e.g. damage to the cooling tube surface area because of prolonged exposure to high temperatures).

Measuring points In order to obtain the flue gases from the furnace, several points have been created from which the gases can be extracted. This allows for direct extraction from each of the burners (E3, E5, E6, E8), the stack, the flue gas circulation pipe (before and after the inducer fan) and from the Species Probe (Section 3.3), see Figure 3.3.
Prior to 2013 only the stack and flue gas extraction points were available. Because the phenomena of increasing oxygen concentration in the flue gas lines and local fluctuations from specific burners were still unexplained, new points were installed before the inducer fan and on all of the burners, as can be seen in Figure 3.3. The point before the inducer fan was chosen because the fan was thought to suck in additional air as a temperature protection mechanism of the fan, resulting in an

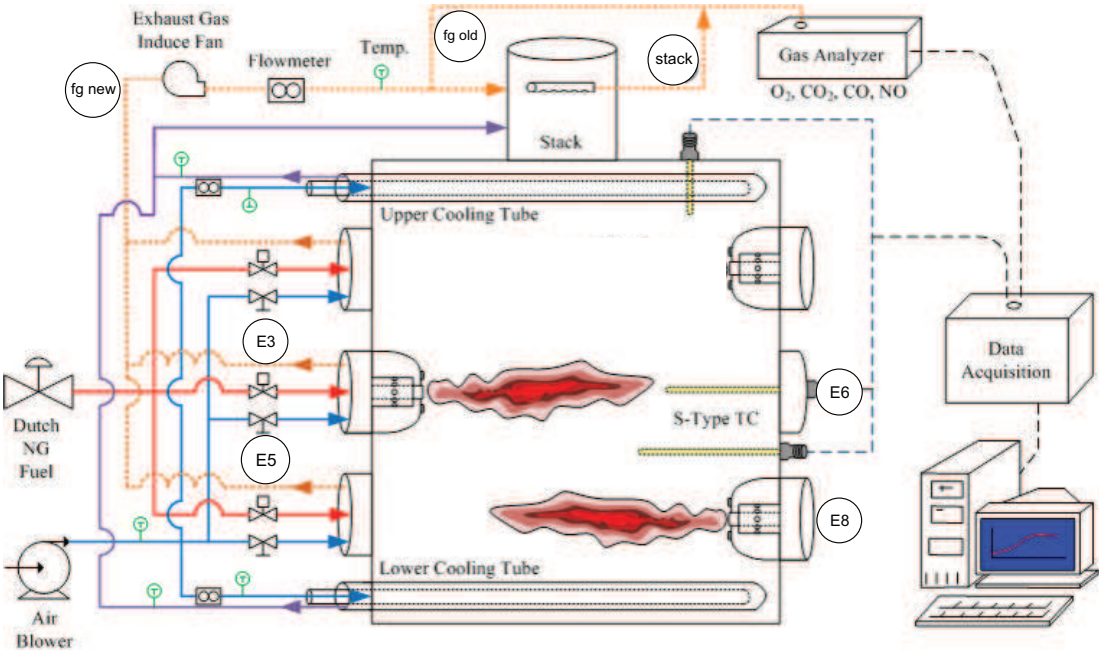

Figure 3.3: Overview of the furnace, where the measuring points have been indicated as circles. The species probe point has been omitted for the sake of clarity of the picture. Image adjusted, original made by E.S. Cho.

increase of O_2 in the flue gas measurements, see Figure 3.4. The location of the new measure location is assumed to not be affected by non-perfect development of the flow streams, see Figure 3.4.
Experiments have been conducted in order to verify this theory. Additional information about the data used can be found in Section 4.4 and the results of the comparison will be shown in Section 6.5.

3.2 Peripheral equipment

Besides the furnace itself additional equipment is present to control and measure the desired parameters. In this section an overview of the flow meter, gas analyzer and species probe can be found.

Flow meter

A recent addition to the setup is the Krohne DK800 flow meter [4] which allows for adjustment of sample gas flow and maintains a constant flow rate ($\approx$ 2.5% accuracy) to the gas analyzer. The operating principle is based on a float measurement in which a floating ball can freely move up and down in a glass cone. It

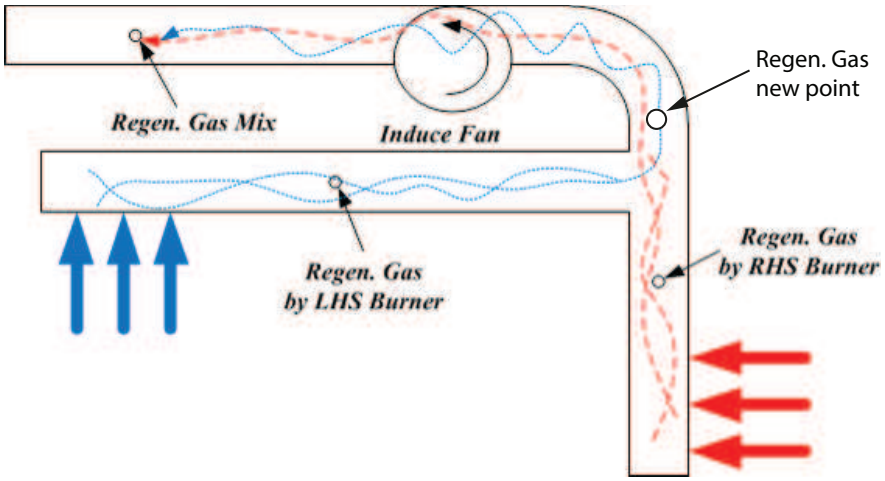

Figure 3.4: This figure shows the situation for the flue gas streams around the inducer fan as well as the new measurement location. Figure adapted from E.S. Cho.

is calibrated to show a flow speed depending on the net force acting on the ball which is a function of the buoyancy force, the form drag and its weight.
Installation was done in order to accommodate the gas analyzers requirement to receive a stable flow of sample gas. This dependency will be discussed in the next section. The flow meter has the ability to limit and control the incoming gas stream in the range of $0-100Nl/\text{min}$ and was set to $0-60Nl/\text{min}$ as default during the experiments. This is in accordance with the specifications of the gas analyzer.

Gas Analyzer

For measurements in the MEEC furnace, sample gas can be collected from several ports, ranging from all of the burners to flue gas streams and the species probe. The gas is sucked in by a pump and then fed to a AGT MAK10 [5] sample gas conditioner which removes the remaining water from the gas. In the last section of the line the gas moves to the analyzer where it is analyzed using a nondispersive infrared (NDIR) sensor.

Analyzer Modules The gas analyzer which has been used is the Sick Maihak S710 [6] and features two installed modules for the detection of sample gas. The first module is the MULTOR for detection of CO, NO and CO_2 by nondispersive infrared absorption. The second module is the OXOR-P for detection of O_2. This is done by a rotating diamagnetic dumbbell, which is suspended in an inhomogeneous magnetic field. The paramagnetic characteristics of oxygen exerts torque

on the dumbbell which is proportional to the concentration of O_2 in the sample gas [7]. The main advantage of this technique is its lack of thermal property dependency of the sample gas combined with a fast response time. Main disadvantage is that it includes moving parts and is thus susceptible for vibrations. However, vibrations are of no concern for the application near the furnace.
Measurement ranges of both modules can be seen in Table 3.1.

Table 3.1: Sick Maihak S710 module operating ranges with accuracy tolerances.

	CO [ppm]	NO [ppm]	CO2 [vol%]	O2 [vol%]
MULTOR	0 - 200 ± 7	0 - 200 ± 7	0 - 10	-
OXOR-P	-	-	-	0 - 25 ± 0.5

Mechanical workings The S710 is equipped with a mechanical chopper. This is a rotating disc with several optical filters installed. A specific filter will be installed for every component that can be measured. This means that only one component can be measured at any given moment. This effectively results in a non-continuous sampling rate when looking at one specific component. The rotational frequency of the chopper ultimately determines the introduced delay for this part of the system.
The mechanical design of the analyzer also requires the feed stream of sample gas to be constant and without large pressure fluctuations. To accommodate for this, the flow regulator was installed as described earlier.

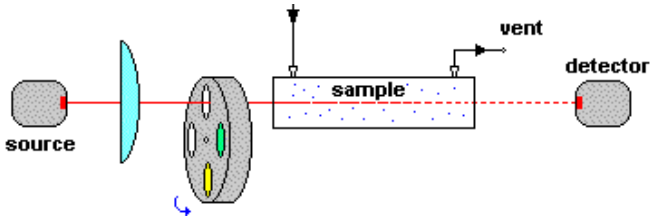

Figure 3.5: Basic representation of the working principle of the NDIR detection method [8].

Nondispersive infrared (NDIR) principle As explained in the previous paragraph, the chopper consists of a set of optical filters, see Figure 3.5. These filters are necessary for the chosen method of gas detection, NDIR. This method is based on absorption of infrared light, which is species specific. Each component in the sample gas has an unique attenuation at specific wavelengths. So when

the source of the gas analyzer sends out all required wave lengths, the filter then only lets through one wave band at a time. The detector at the other side of the sampling probe then measures the fraction of absorbed light and can thus measure the concentration of a certain component in the sampling gas.
The main difficulties with this technique are twofold. The first problem might be the just described modulation that cannot be circumvented without using multiple dedicated sampling gas chambers. This is not an option in the current setup so it is a factor to take into consideration.
The second problem is cross-interference of different components in the infrared spectrum (780nm - 1000nm). As mentioned before each molecule should have a unique wavelength at which a maximum absorption is achieved. However in practise this is not always the case. For instance the absorption bands of CO_2 and H_2O overlap for certain wavelengths. This could potentially result in falsely detecting CO_2 when in fact H_2O has absorbed part of the light or vice versa. This phenomena is particularly important in relation to the MEEC furnace where CO_2 and H_2O are both present as combustion products. To prevent this from happening, the gas analyzer is equipped with internal cross-sensitivity compensation software that can compensate for an occurring interfering effect. The algorithm of the gas analyzer uses factory calibrated zero-point values and because the zero-point values drift over time the internal cross-sensitivity of the gas analyzer should be calibrated once a year (manufacturer advise) to prevent cross-interference of mainly H_2O with CO_2.

Measuring value computation The Sick Maihak S710 gas analyzer has some additional settings which users can set themselves. These settings are related to the way the analyzer computes the detected signals. From the User Manual [9] two types of damping are described: average value and dynamic. Average value damping works as a moving average and can be manually adjusted for each measuring component from $0,5s - 20s$ (default = 15s). Removing this filter will reduce the delay time but might increase measuring noise.
The dynamic damping detects rapid changes in the measuring values and turns off when the threshold value is exceeded by more than $(0\% - 10\%)$, within a specified timescale $(1s - 120s)$. The dynamic damping is turned on, when no rapid changes are detected in the measuring value, to "smooth out" continuous minor fluctuations of the measuring value. Again, this setting can be activated for each measuring component individually.
NB: The existence of these settings have not been generally known within the research group so with a high probability one can say that all experiments up till and including those done in 2013, are with both settings enabled and set to

default. The measurements from 2014 have not used the default settings, resulting in choosing the minimum damping possible by the gas analyzer to minimize the added transient delay of the gas analyzer.

Mass Flow Controller

To simulate biofuels, addition of either the regular CO_2 or N_2 is required to the DNG stream. The supply of the diluting streams is controlled by two F-203AV-1M0-RAD-55-V mass flow controllers from Bronkhorst B.V. which have a range of 20/1000ln/min for N_2 and 18/900ln/min for CO_2. However, a characteristic of the controller is the slow settling time (2-4s) which make these mass flow controllers not suitable for rapid switching of the flow rate following the cycle time of the furnace. What they can do very well is maintaining a constant flow rate. The problems that arise with use in the current system will be further discussed in Section 3.4.

Thermocouples

Measurement of temperatures in the MEEC furnace is performed by several TMG S-type thermocouples [10]. These thermocouples are located at a number of locations throughout the furnace. The measuring range is $0 - 1300°C$ with an accuracy of $\pm 1K$.
Burner exit temperatures are measured with TMG K-type thermocouples [11] over a range of $0 - 1000°C$ with an accuracy of $\pm 4K$.

3.3 Species Probe

Based on prior research into flameless combustion [3] it was recommended to further investigate the species components in the furnace by way of extractive measurements. The species probe, shown in Figure 3.6, was deemed the device best suited for this application. In the next couple of paragraphs more information regarding the species probe design and operating method will be discussed.

Design Design and production of the species probe began in late 2012 and was completed around the summer of 2013. The probe is a continuously water cooled (30 - 40 l/min) stainless steel tube with an opening through which the flue gases can be transported as can be seen in Figure 3.6. The length of the species probe is slightly more than the length required to reach the burner nozzle while still having enough room to manoeuvre from the outside of the furnace.

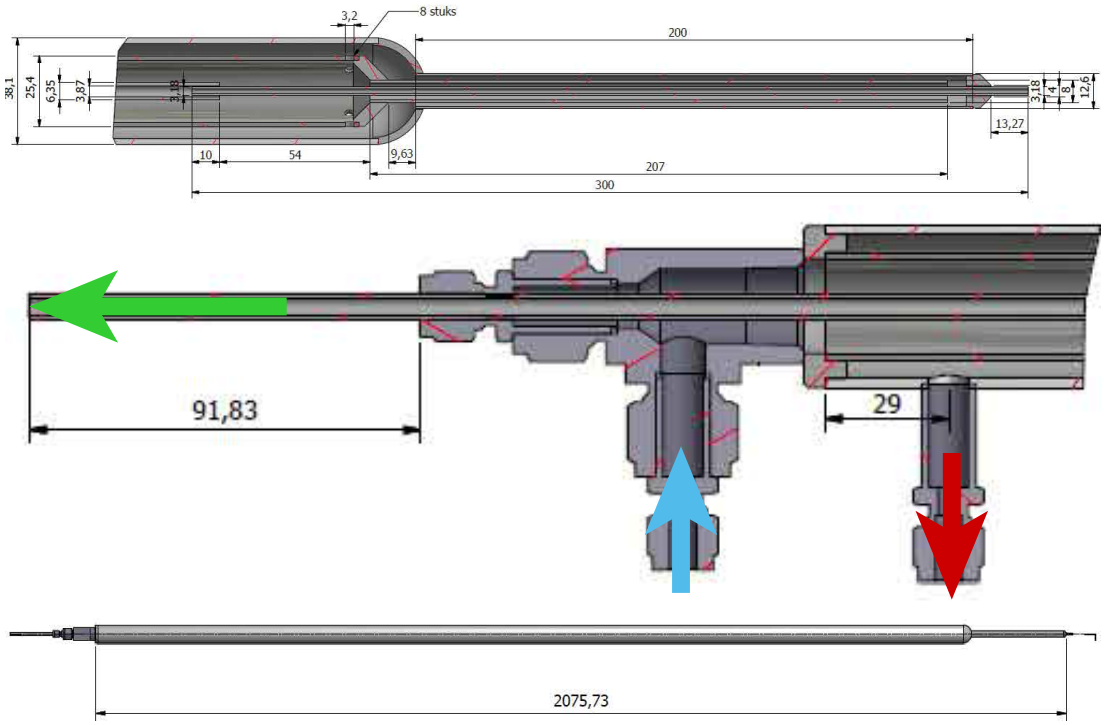

Figure 3.6: Technical drawings of the species probe with a magnified view of the top (top) and end (middle) sections and a global view (bottom). All dimensions in mm. Flows of flue gas (green) and water in & out (blue, red) are shown in the middle picture.

One of the goals of the probe was to verify and visualise a near-burner combustion zone in a large scale furnace such as found at the DUT. Previous research [12] showed details of a near burner zone in small-scale setups. In order to successfully validate CFD models, measurements had to be conducted along a line opposite to the burner, see Figure 3.7.

Operation Each time the species probe was used in an experiment, a fixed insertion procedure ensured that the results between multiple experimental days would be comparable. A summary of the steps followed is given here:

1. Start furnace operation and feed water stream for water cooling of the species probe.
2. Alignment of the tip to the opposing furnace wall (usually already executed in step 5).
3. Once a steady-state temperature in the furnace was reached measurements began.

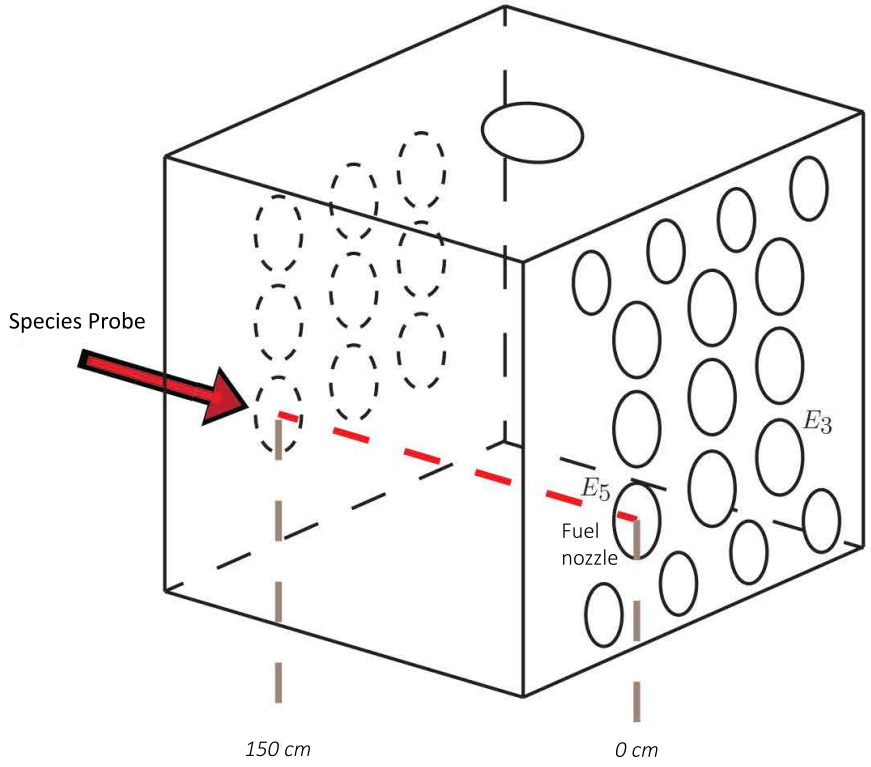

Figure 3.7: Shown here in red is the line along which the species probe is inserted into the furnace from the 150cm mark up until 5cm away from the fuel nozzle.

4. Insertion of the probe to several predetermined positions along the burner axis, see Table 4.2.
5. Experiment finalised with subsequently the extraction of the probe up until it aligns to furnace wall.
6. Turn off furnace and water supply.

3.4 Furnace adaptations

Prior furnace repairs Till the summer of 2013 the furnace had been in maintenance for several months. The insulation had to be replaced to prevent damage from occurring. It was then found that the insulation on top wall was hanging loose from the ceiling. Having loose plates of insulation not only possibly damages the furnace, but it also affects the internal flow patterns and the species concentrations inside due to furnace condition that differ locally which could result in e.g. radical quenching. Not only due to differences in local temperature that affect the reaction but also possibly from reaction of the insulation material

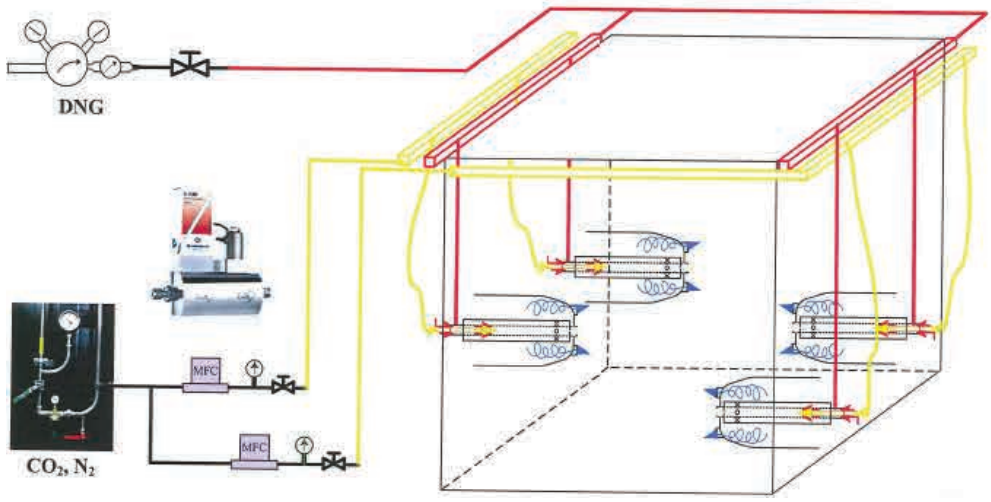

Figure 3.8: Current state of furnace. The red lines show the DNG supply while the yellow lines show the CO_2 or N_2 supply. Figure made by E.S. Cho.

itself. As is known, combustion consists of various radical chain reactions that can be initiated by a single radical. The same holds true for radicals that slow down the reaction or prevent it from occurring (think of addition of lead to gasoline to prevent early ignition in low-pressure conditions). As such, the insulation material can definitely influence the (local) combustion process.

Current situation Current limitations of the furnace have to be overcome by adjusting the system. The setup does not allow for alternating supply of dilution-agent for the simulation of biofuels. Instead the diluting agents (CO_2 and N_2) are continuously fed into both the active and regenerative side of the burners at the same time, see Figure 3.8. The effects on the in-situ species concentrations with such a setup can be large in scope, as it will become more difficult to fully understand where the species (like CO_2) are formed and whether they are the result of injection at the regenerative side or at the active flame side.

System after adjustments In order to improve upon the current installation, several changes will be proposed that enable experiments to be conducted with simulated biofuels. The changes to the system have been summarised in Figure 3.9. Here differences in feed pressure have been taken into account in both the Dutch Natural Gas (DNG) lines as well as in the diluting agent lines (CO_2 or N_2). These streams combine in a static mixer where they are (ideally) mixed. The combined product leaves the mixer and enters the burners via the regular DNG

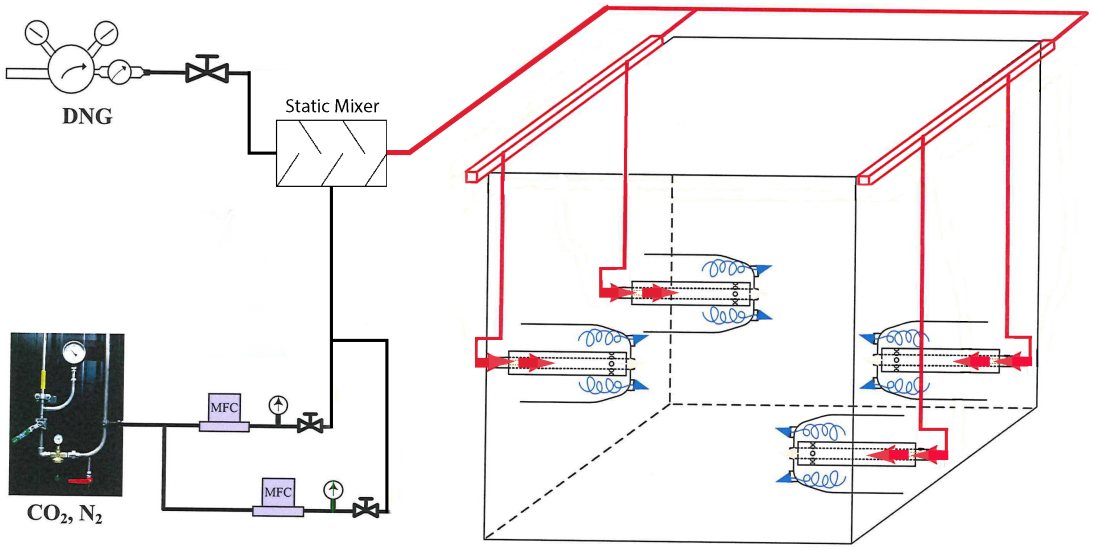

Figure 3.9: This figure shows the suggested system where the dilution streams and DNG are premixed in a static mixer and use the current control system during operation.

lines. The alternating sequence is controlled by the LabView computerprogram which is fully functioning and requires no further adjustments.

3.5 Encountered problems

Problems will turn up when doing experiments. This was also the case during the experimental campaign done for this thesis. A short summary of the "incidents" that occurred will be explained here to illustrate further the difficulty of obtaining trustworthy results in a large scale experimental setup.

Burner air leakage The leakage of air within the burner itself is due to the valves that are not manufactured to be airtight. A representation of what happens can be seen in Figure 3.10. The leakage of air results in difference in mass and heat balances as well as losses in efficiency.

Excess water in flue gases During one of the experiments in Staggered 1 firing mode, see Chapter 4 for firing mode definitions, water was observed in the lines coming from burner E8 which was attached to the gas analyzer at the time. Because of the used setup towards the gas analyzer, only a part of the water could be removed by the sample gas conditioner. The phenomena was detected during measurement but unfortunately it was too late to prevent water damage. The

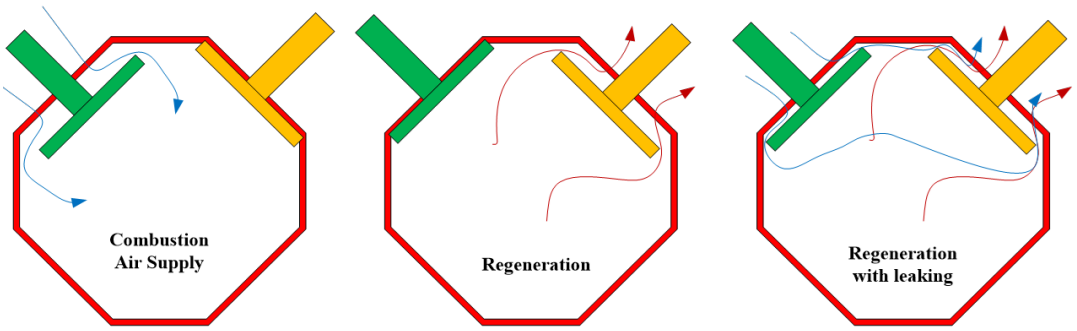

Figure 3.10: This figure shows the pathways of the air through which it can escape *(leakage)* during several steps of the burner cycle. Figure made by E.S. Cho.

condensate had already "drowned" the sample gas conditioner and flooded the gas analyzers internal parts, which by then was displaying an error (condensate). To prevent this problem in the future, a special type of Erlenmeyer flask was added in between the pump and the sample gas conditioner. This allows the condensate to be collected in the flask and the sample gases to pass on to the gas conditioner as normal. The downside of this approach is the added volume in the lines (flask) which will increase the measurement delay and in turn will make it more difficult to interpret the analyzer signals.

Time-delay of measurement During the experimental campaign it was noticed that there was a delay between the actual moment a process took place (i.e. switching of burner cycle) and the moment that the gas analyzer showed a change in its readings. Figure 3.11 is a theoretical representation of the measured delay. The time it took to register a change in the gas analyzers reading was measured after inducing a large CO_2 flow to the inactive furnace. The time it took to change was stable at around 35s.

Unequal cooling air distribution A flow through the cooling tubes can be obtained by setting the valves positions as a percentage of the total (open) situation. The top and bottom sides both have a controller that can be set to a desired setpoint percentage. Internal friction can cause the position of the valve to alter slightly, due to the physical construction of the valves, resulting in a difference between the top and bottom cooling air flow volumes, even when the same setpoint values was used. This led to an unequal flow rate and thus an unequal heat extraction for the top and bottom sides. This is not a big problem in itself as long as it is known, as it is a boundary condition for the CFD models (see Chapter 5), but in the past this was not taken into account. In fact, the

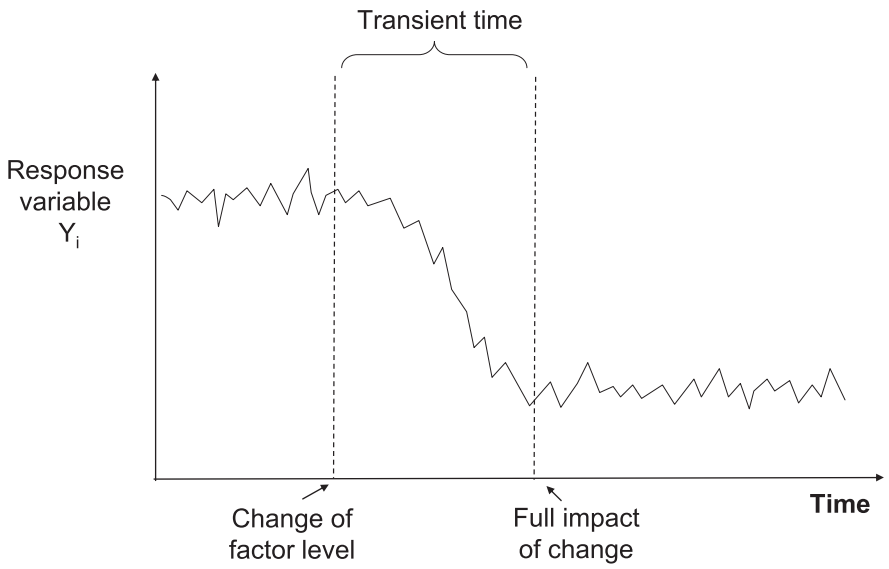

Figure 3.11: This is an illustration of the transient time required during continuous processes such as in the MEEC furnace before an induced change to the system is stabilized in the response [13].

difference was believed to be partly the cause of convection effects in the furnace itself [14].
After opening the valve controllers and seeing that not much could be changed, it was decided to change the way of controlling the flow instead. All experimental results in this thesis have been obtained by matching the sum of the flow rates of the top and bottom cooling tubes to a fixed total flow rate as desired for the specific experiment with 50% of the flow diverted to both the top and bottom side. In the past the percentage setpoint was used instead of the actual flow, resulting in unequal flows for the top and bottom sides of the cooling tubes.

References

1. Ceramics, T. Insulating firebricks jm: Product information (2006).
2. Ceramics, T. Superwooltm 607tm ht blanket: Product information (2006).
3. Danon, B. *Furnaces with multiple flameless combustion burners.* Ph.D. thesis, Delft University of Technology (2011).
4. Krohne. Dk46 - dk800: Technical datasheet (2014).
5. AGT Thermotechnik, G. Operating manual: Mak 10 sample gas conditioner (2007).
6. Maihak, S. S700 modular gas analyzer system: Product information (2003).
7. Sanner, B. Paramagnetic: Principle of operation. *http : //biomed.eti.pg.gda.pl/ bartek/4_en.html* (2006). [Online; accessed 11/03/2014].

8. Services, K. E. E. Non-dispersive infrared and gas filter correlation. `http://www.k2bw.com/` (2014). [Online; accessed 24/03/2014].
9. Maihak, S. S700 modular gas analyzer system: User manual (2003).
10. TMG. Thermoelement typ tp 10 (2006).
11. TMG. Mantelthermoelement typ mo 73 (2006).
12. Riahi, S., Roekaerts, D. J. E. M. & Lupant, D. Numerical comparative study of heat transfer in flameless and conventional combustion in a 30 kw furnace. In *Proceedings of the European Combustion Meeting* (2013).
13. Vanhatalo, E. *Contributions to the use of Designed Experiments in Continuous Processes: A Study of Blast Furnace Experiments*. Ph.D. thesis, Luleå University of Technology (2007).
14. Cho, E. S., Shin, D., Lu, J., de Jong, W. & Roekaerts, D. Configuration effects of natural gas fired multi-pair regenerative burners in a flameless oxidation furnace on efficiency and emissions. *Applied Energy* **107**, 25–32 (2013).

Chapter 4

Experiments

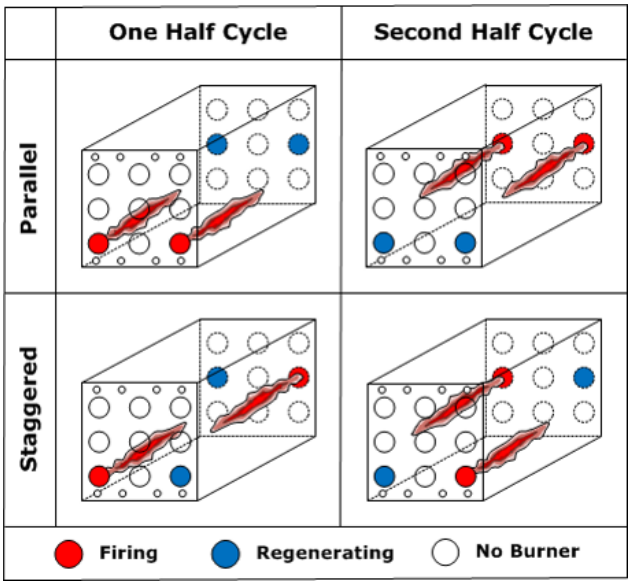

Figure 4.1: Overview of the firing modes used. The parallel mode is shown on top for both parts of the cycle and the staggered 1 mode is shown on the bottom.

4.1 Experimental campaign

Since the construction of the MEEC furnace, experiments have been conducted using a wide spectrum of possible settings and configurations [1, 2]. The focus of these experiments has, for the most part, been to find out in what way the chosen burner configuration and firing modes resulted in differences in performance (emissions, temperature uniformity, cooling tube efficiency etc) and to validate CFD models.

The campaign executed for this thesis consisted of several measurements that were already done in the past, because the conditions of the furnace were anticipated to be improved after recent repairs, see Section 3.4. This data could also function as an improved reference case to further experiments with a simulated biofuel which are planned for the near-future.

The criteria on which the selection of "best" or "optimal" burner configuration and firing mode was based, were the cooling tube efficiency (as high as possible), cycle time (effect on emission and temperature uniformity) of the burners, excess air flow rate (emission effect and temperature) and emissions (as low as possible). From these experiments, the burner configuration was chosen as seen in Figure 4.1 and two firing modes (parallel and staggered 1). For more information regarding the complete set of tested burner configurations and firing modes, see B. Danon [2]. The configurations that were used for this thesis can be seen in Table 4.1.

Table 4.1: Overview of the experiment. Different firing modes have been selected for a changing cooling air flow rate and vice versa. In the burner configuration column an overview of the active (1) and regenerating (2) burners can be seen. These alternate after a set cycle time (30s). The lower section of this table gives an overview of the used data files for the graphs in Chapter 6 with a special addition for the flue gas (FG) measurement.

Burner Configuration	**Firing Mode**		**Combustion Air** (m^3/h)	**Cooling Air** (m^3/h)
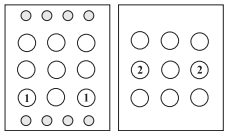	Parallel		105 - 125	250 - 600
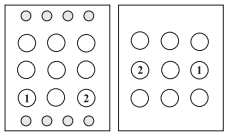	Staggered 1		105	360 - 600
		Days		
	Parallel	20130904	105	360
		20130920	110	360
		20130913	115	360
	(FG compare)	20130925	120	360
		20130905	125	360
		20131106	105	250
		20130904	105	360
		20130904	105	450
		20131107	105	550
		20131108	105	600
	Staggered 1	20130926	105	360
		20140205	105	450
		20140206	105	550
		20140207	105	600

4.2 Firing mode

Out of the many possible physical arrangements of different burner locations, one was selected that had the best performance [2]. In the chosen configuration, as seen in Figure 4.1, differences can be introduced in the sequence of firing and regenerating. Again, the most promising combinations were selected for further investigation. This has led to the selection of C4-II-Parallel and C4-II-Staggered-1. A third case, the C4-II-Staggered-2 case, featured two active burners that were

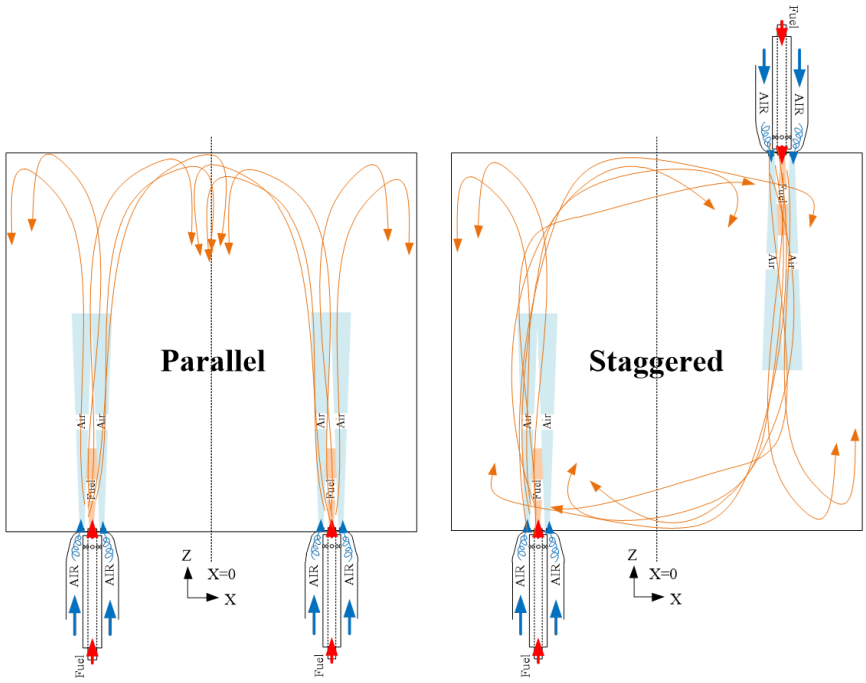

Figure 4.2: Theoretical 2D flow patterns in the furnace during the parallel and staggered firing modes. Figure made by E.S. Cho.

on the same axis but on opposing sides. This case was omitted in the current study, due to the low cooling tube efficiency (Appendix A) and relatively high formation of CO and NO.

4.3 Flow patterns

Changing the firing mode of the furnace will also induce different flow patterns in the furnace. A representation of phenomena is shown in Figure 4.2. The change in flow pattern causes the pathway of the flue gases to change. In the case of the Staggered 1 firing mode, the pathway along which the flue gases travel will shorten for a certain fraction of the internal flue gas stream. This could be the result of gases hitting the opposing side of the furnace and then travel directly to the regenerating burner below/above. Or this could happen due to short-circuit suction of flue gases by the burner that is located in the same wall as the firing burner. As a result the residence time in the furnace will change and as such, differences in species concentrations are expected to show up in the results of the species probe measurements, see Chapter 6.

4.4 Species Probe

During the above described variations of the setup, data has been collected using the species probe. For each configuration a set of insertion depths has been selected for data collection. The chosen points have a higher resolution (closer

Table 4.2: This table gives a complete overview of the species probe location that have been used for the data as seen in Table 4.1. A graphical view of the species probe insertion can be seen in Figure 3.7.

	Species Probe location (distance to fuel nozzle in cm)													
Days	**5**	**10**	**15**	**22**	**26**	**30**	**34**	**38**	**45**	**60**	**75**	**100**	**125**	**150**
20130904	✓	✓	✓	✓	✓	✓	✓	✓	✓	✓	✓	✓	✓	✓
20130920	✓	✓	✓	✓		✓		✓	✓	✓	✓	✓		✓
20130913	✓	✓	✓	✓		✓		✓	✓	✓	✓	✓		✓
20130925	✓	✓	✓	✓		✓		✓	✓	✓	✓	✓		✓
20130905	✓	✓	✓	✓	✓	✓	✓	✓	✓	✓	✓	✓	✓	✓
20131106	✓	✓	✓	✓		✓		✓	✓	✓	✓	✓		✓
20130904	✓	✓	✓	✓	✓	✓	✓	✓	✓	✓	✓	✓	✓	✓
20130904	✓	✓	✓	✓	✓	✓	✓	✓	✓	✓	✓	✓	✓	✓
20131107	✓	✓	✓	✓		✓		✓	✓	✓	✓	✓		✓
20131108	✓	✓	✓	✓		✓		✓	✓	✓	✓	✓		✓
20130926	✓	✓	✓	✓		✓		✓	✓	✓	✓	✓		✓
20140205	✓					✓				✓		✓		✓
20140206	✓					✓				✓		✓		✓
20140207	✓					✓				✓		✓		✓

together) in the zone close to the burner. This was chosen because more information in this near-burner region is required to validate the CFD models. Not all of the data sets feature the same amount of points, however, because of the time required for an experiment. Due to the long heat up cycle of the furnace, see Appendix B, not much time is available per day and the individual measurements per point take up 10 minutes. After the results of the first couple of days came in, it was concluded that less resolution was required in certain areas, as can be seen in Table 4.2.

Regenerative flue gas comparison The regenerative flue gas composition will be studied, from the new measurements location before the induce fan, and compared with the old location, as mentioned in Section 3.1.

References

1. Cho, E. S., Danon, B., de Jong, W. & Roekaerts, D. J. E. M. Behavior of a 300kwth regenerative multi-burner flameless oxidation furnace. *Applied Energy* **88**, 4952–4959 (2011).
2. Danon, B. *Furnaces with multiple flameless combustion burners.* Ph.D. thesis, Delft University of Technology (2011).

Chapter 5

Computational Fluid Dynamics

5.1 MEEC furnace: three cases

The CFD simulation of the MEEC furnace will be explained here, based on the settings that are available in the commercial package Ansys FLUENT. Version 6.3 was used for the case of A. Jansen [1] and version 12.0 for the cases of D. Shin [2]. The most influential factors on the outcome of the simulations are the amount of detail of the mesh (number of cells), the type of solver and the material properties. Furthermore, the selected models are of great importance: turbulence, chemistry, turbulence chemistry interaction, radiation, NO_x chemistry.
Apart from explaining the settings of the models, a comparison between two [2, 1] simulation studies will be made in this chapter in terms of settings used. These two simulation outcomes will be compared with the profiles of measured flue gases inside the furnace in Chapter 6.
For easy referencing a table was created for the selected simulated cases, see Table 5.1.

Table 5.1: This table summarizes the selected cases that will be used as comparison for the results as obtained from the species probe experimental campaign. All cases feature a cooling air flow similar to 250 m^3/h and a burner air flow rate of 105 m^3/h.

	D Shin		**A. Jansen**
Case Number	**1**	**2**	**3**
	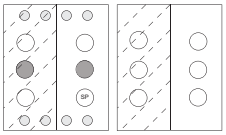	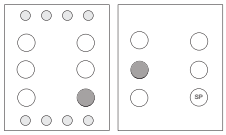	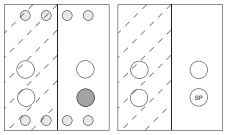
Fuel	DNG	DNG	DNG
Firing mode	parallel	staggered 1	parallel
Mesh (cells)	591056	1005648	462024
Part of furnace	half	all	half
Radiation	DO	DO	DO
Species	smooke (19)	smooke (16)	smooke (19)
Turbulence	real. k-ϵ	real. k-ϵ	real. k-ϵ
NOx	Thermal Prompt N2O	Thermal Prompt N2O	Thermal Prompt N2O + reburn

Mesh The mesh over which the simulations are executed is a modelled approximation of reality using a wire frame structure. This structure consists of hexahedral cells which are distributed over the mesh over a number of different zones. Each zone is specifically tailored to the type of surface structure it has

to describe. More detail (smaller hexahedral cells) can be obtained for a zone in which a higher resolution is desirable, i.e. bends, nozzles or rounded surfaces such as cooling tubes or reaction zones by adding smaller cells.
For the case of A. Jansen the mesh consists of 462.024 cells for half of the furnace, using the axis domain symmetry to reduce computational costs. In this mesh only two burners on each side are modelled, which is no problem because the configurations used, see Chapter 3, do not require the top burners to be modelled. Due to prior parameter optimization by B. Danon it was concluded that the optimal burner configuration was the one chosen in Chapter 3. The furnace allows placements of burners on three level of heights, however, the top position was not found to result in optimal operating conditions.
The parallel case that was created by D. Shin [2] uses a different mesh than that of A. Jansen. In fact, it was created to be more precise by adding more cells in critical areas. The mesh is built up by 591056 cells for half of the furnace.
The mesh for the staggered 1 case by D. Shin features the whole furnace because the furnace is not symmetrically operated. Because of the furnace being asymmetrically fired the mesh also has almost twice as many cells but it still has the same amount of detail in the mesh.

Turbulence All of the cases that will be compared in this study make use of the realizable k-ϵ model as used in FLUENT [3]. This is an adaptation of the standard k-ϵ model for round jets. In the case of large scale furnaces such as the MEEC, the realizable k-ϵ model is expected to give better results for a relatively small increase of computational time.

Species The reaction chemistry is modelled by the Smooke46 [4] mechanism in all cases. This mechanism consists of 16 or 19 species with 46 reactions. This mechanism is combined with the eddy-dissipation-concept (EDC) [5] model (default parameters) for the modelling of the turbulence-chemistry interaction.

Radiation The default discrete ordinate (DO) radiation model has been used for all of the cases. This model describes the radiative transfer equations and is combined with the domain based weighted sum of gray gases model (WSGGM) for the absorption coefficient of the gas mixture.

References

1. Jansen, A. *Numerical study on a multi-burner flameless oxidation furnace in relation to change in fuel composition.* Master's thesis, TU Delft (2012).

2. Cho, E. S., Shin, D., Lu, J., de Jong, W. & Roekaerts, D. Configuration effects of natural gas fired multi-pair regenerative burners in a flameless oxidation furnace on efficiency and emissions. *Applied Energy* **107**, 25–32 (2013).
3. FLUENT, A. Fluent 6.3 user's guide (2006).
4. Smooke, M. D., Puri, I. K. & Seshadri, K. A comparison between numerical calculations and experimental measurementss of the structure of counterflow diffusion flame burning diluted methane in diluted air. *Twenty-First Symposium (International) on Combustion* **21**, 1783–92 (1986).
5. Ertesvåg, I. S. & Magnussen, B. F. The eddy dissipation turbulence energy cascade model. *Combustion Science and Technology* 213–235 (2000).

Chapter 6

Results & Discussion

6.1 Introduction

In this chapter an overview of the obtained results from the experimental campaign as well as the results from the CFD modelling will be shown. Each of the selected campaigns in Chapter 3 will be reviewed in terms of the temperature, species concentrations and several other parameters. Lastly, these results will also be compared in the interest of answering the research questions whether or not the species probe measurements can be succesfully executed in such a way that they can be used to validate the CFD model.
It should be noted that the data shown here are whole cycle averaged values over a number of complete burner cycles. This means that the numbers are averaged over the course of four complete cycle times. Hence, it is impossible to distinguish individual cycles of regeneration and firing mode due to the averaging among other things. More information regarding the precise data analysis can be found in Appendix A.

6.2 Cooling air - Parallel

Temperature Figure 6.1 shows the temperature uniformity in the furnace and the temperature of the furnace itself. These are both a function of the distance of the species probe that is inserted into the furnace. The temperature plot shows the distribution of the temperature, here the lowest temperature is measured for the case of the highest cooling air flow rate. The other cooling air flow rates are distributed with increasing temperature for decreasing cooling air flow rates.

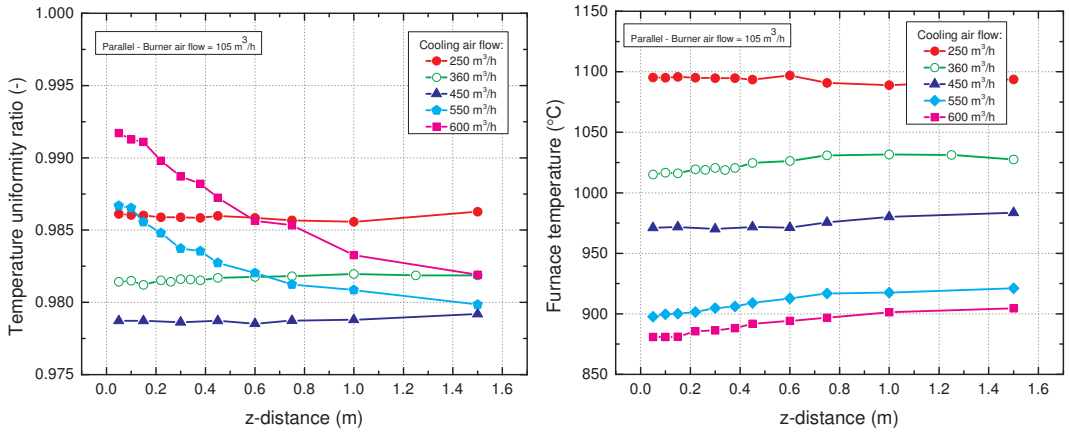

Figure 6.1: Parallel firing mode. The temperature uniformity (left) and furnace temperature (right) for several cooling air flow rates and constant burner air flow rate are shown as a function of species probe insertion depth. Burner is located at $z = 0$.

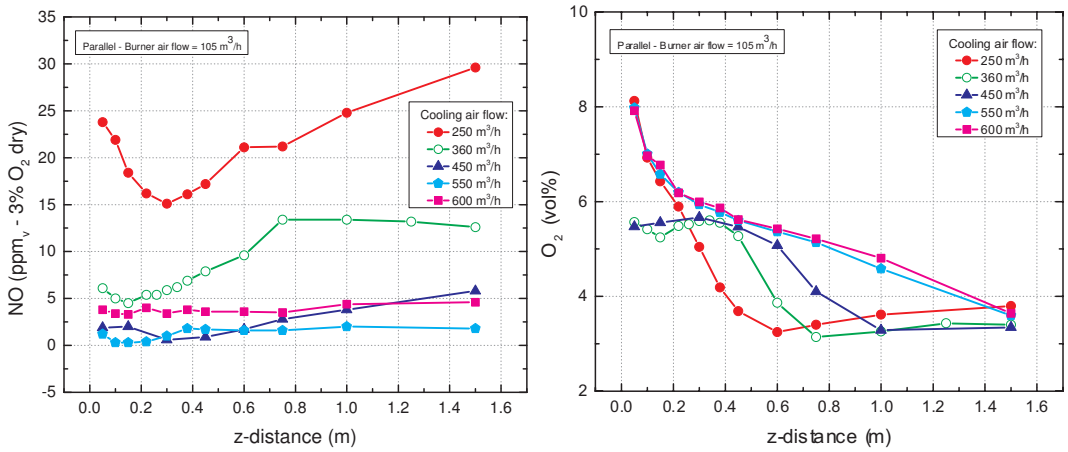

Figure 6.2: Parallel firing mode. On the left the NO concentration is shown as a function of species probe insertion depth for several cooling air flow rates with constant burner air flow rate. The oxygen concentration can be seen on the right for the same cases. Burner is located at $z = 0$

A different result can be seen in the plot for the temperature uniformity in the furnace. Two of the measured data lines show an increase of temperature uniformity for insertion of the species probe. This is odd, due to the fact that the species probe is water cooled and is thus not expected to introduce a balancing effect on the temperature uniformity. A possibility could be the significant change in temperature of the furnace itself due to the cooling capacity of the furnace combined with the species probe. Lowering the global temperature of the furnace then results in local temperature fluctuations having an increased effect on the temperature uniformity in an absolute sense. Worth noting is that the temperature measurement of the furnace is done by a set of thermocouples situated in the furnace walls. These are used for determination of the difference of each thermocouple, see definition of the temperature uniformity (Appendix A), and are located on the same side of the furnace as the species probe. This might also be a cause of the relatively high uniformity of the furnace for complete species probe insertion, especially during the 550 m^3/h and 600 m^3/h cooling air flow rates where the global temperatures are the lowest.
The effect of the insertion of the species probe can also be seen from the temperature graph. The data lines show a drop in furnace temperature ($\Delta T \approx 20°C$), which results in combustion at lower temperature, when the probe is inserted into the furnace. The ΔT is higher for the furnace temperatures that correspond to higher cooling air flow rates then for for lower cooling air flow rates.

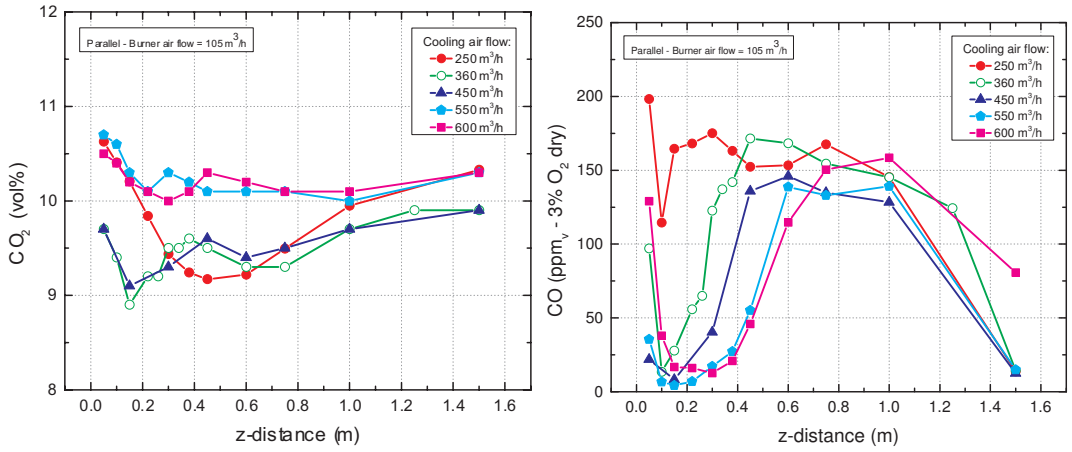

Figure 6.3: Parallel firing mode. In the left graph the species concentration for CO_2 is displayed as a function of species probe insertion depth for several selected cooling air flow rates. On the right the CO concentration is shown for the same cases. Burner is located at $z = 0$

Species concentrations When looking at figures for species concentrations such as NO, CO and CO_2, one has to always take into account the amount of oxygen because the measured values are normalised to 3% O_2 (Appendix A). Figure 6.2 shows an overview of the oxygen and NO values as measured. As expected from theory the oxygen data lines show similar trends with more oxygen in the regions closer to the burner than in regions further away. Data lines for 360 m^3/h and 450 m^3/h show a small "hill" type curve near the burner, possibly indicating the near burner zone. However, these two data lines were collected in a measurement that was held on the same day. Therefore the possibility of day-to-day variation effects cannot be ruled out.
The near burner zone concentration profile of NO can be seen for the 250 m^3/h cooling air flow rate in Figure 6.2 with higher NO being measured compared to the other lines. This is in accordance to the higher temperature (1100°C) in the furnace during the experiment as described in the previous section. The case of 360 m^3/h shows a slightly increased NO formation at the temperature of roughly 1025°C. which is in accordance with the theory of NO formation also. As for the other data lines (450 - 600 m^3/h) the results show low values indicating concentrations of 0 - 10 ppm at 3% O_2. Considering the accuracy of the gas analyzer ($\pm 7ppm$) it is safe to say that hardly any NO is present in these cases which relate to temperatures of 975°C and lower.
Looking at the CO graph (Figure 6.3) a distinguishable region can be identified as near burner zone. Ranging from 5 - 38 cm the concentration of CO diminishes where the reaction zone is fully established with the minimum concentration

between 10 - 30 cm. In this area it is probable complete combustion takes place resulting in less CO production. A notable trend can be observed in the data lines of the CO graph, as increasing cooling air flow rates result in an axial offset along the x-axis. Thanks to a higher temperature in the furnace the reaction kinetics become faster and this results in a higher CO measurement value close to the burner nozzle. However, contrary to the other lines for cooling air flow rate, the line for the 250 m^3/h case shows a relatively high CO concentration just after the burner nozzle. This might indicate there are very high local reaction kinetics resulting in sub-stoichiometric combustion.
Further away from the nozzle, the CO values rise again. This trend can be directly related to the local oxygen concentration, see Figure 6.2. The oxygen in the region of the near burner zone is sufficient for complete combustion, however, the concentration drops further away from the burner nozzle, resulting in more CO production due to a sub-optimal oxygen supply for the combustion reaction. At the opposing wall of the furnace, the CO concentration drops again, because more CO has been converted to CO_2.
The Boudouard reaction could also play an important role in the conversion of CO into other products, resulting in a decrease of (local) CO concentration. More information regarding the Boudouard equilibrium reaction can be found in Section 6.7.
An important difference in the CO_2 graph is the lower concentration for the 360 m^3/h and 450 m^3/h data lines. This cannot be directly explained, however it might be related to the lower oxygen concentration, resulting in fewer CO that is being converted into CO_2, see Figure 6.2.

Cooling Tube Efficiency and Regeneration ratio The cooling tube efficiency can be seen in Figure 6.4. The data lines are more or less horizontal and as expected are a function of the cooling air flow rate, meaning more heat is extracted for a higher cooling capacity. The lines for the cases 250 - 550 m^3/h drop slightly when the species probe is inserted into the furnace, because less heat is then extracted by the cooling tubes due to the addition of another heat sink. In the case of 600 m^3/h this drop is hardly noticeable, probably due to the high cooling air capacity itself.
The regeneration percentage is shown in the graph to the left in Figure 6.4 and shows a remarkably high percentage for the cases 360 m^3/h and 450 m^3/h. Apart from the fact that the data for these two lines were collected on the same day, see Table 4.1, there are no indications as to why the rate is so much higher.

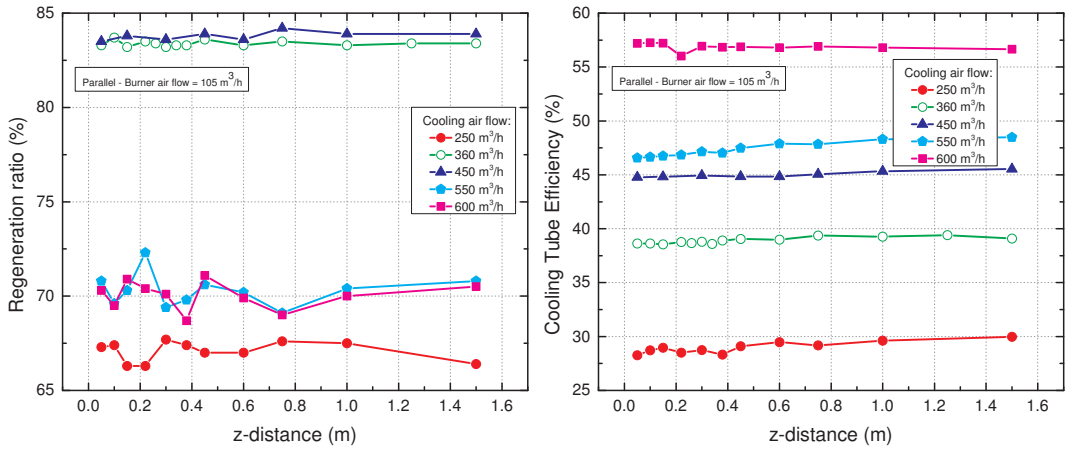

Figure 6.4: Parallel firing mode. The regeneration rates (left) and cooling tube efficiencies (right) as a function of species probe insertion depth for varying cooling air flow rates are shown in this figure.

6.3 Cooling air - Staggered 1

Temperature Figure 6.5 shows the temperature uniformity and global temperature of the furnace as measured during the Staggered 1 firing mode. The lines for the temperature of the furnace show nothing truly remarkable and show the same trend with species probe insertion as previously explained in Section 6.2 involving parallel firing mode. The temperatures are not much higher than the threshold for flameless operating mode (Appendix B) for the cooling air flow rate of 550 m^3/h and 600 m^3/h which should result in relatively low NO and

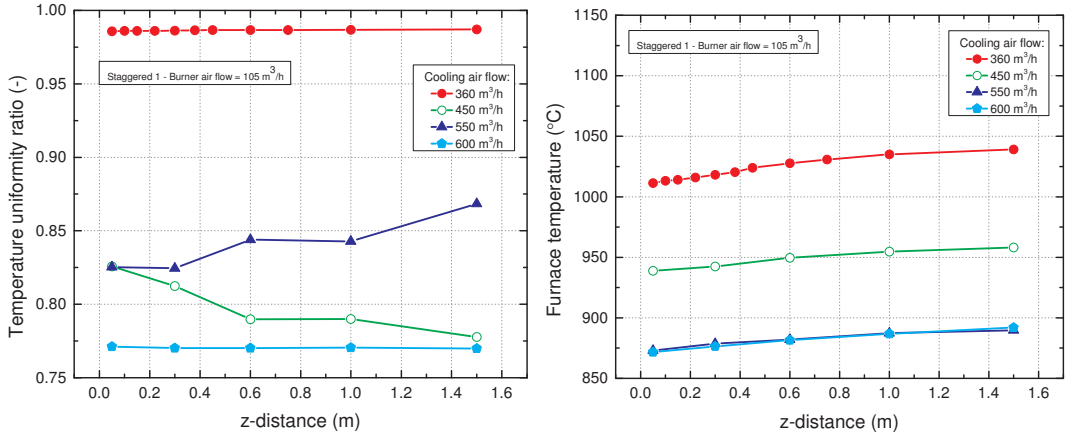

Figure 6.5: Staggered 1 firing mode. This figure shows the temperature uniformity (left) and furnace temperature (right) as a function of species probe insertion depth for varying cooling air flow rates.

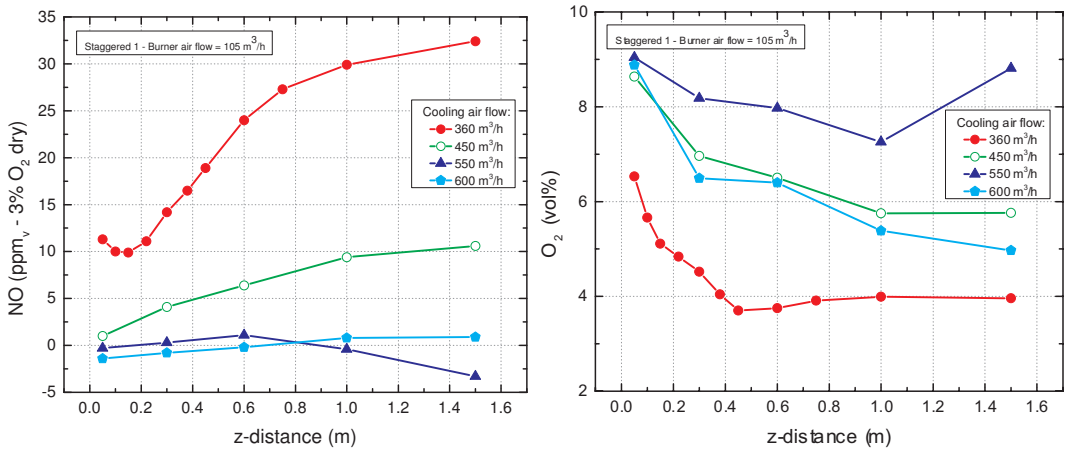

Figure 6.6: Staggered 1 firing mode. NO and oxygen concentration are shown on the left and right in this figure. Both are displayed as a function of the insertion depth of the species probe for several cases of cooling air flow rate.

high CO formation, see Section 1.2.
The temperature uniformity tells a different story, however, as there are discrepancies between the measured data sets. The uniformity of both the 360 m^3/h and the 600 m^3/h cases stay constant regardless of the insertion of the species probe. The 360 m^3/h data set is in the same range as the ones we have discussed in Section 6.2 while the others are significantly lower. The cause of this phenomena might lie in the changed flow patterns in the furnace while also having a lower global temperature in the furnace. Considering larger differences due to a different flow pattern it seems that a higher global temperature results in a smaller effect of the flow inside on the temperature uniformity. In terms of heat distribution and heat fluxes from the walls the case in which the furnace is at a higher temperature will feature a more uniform temperature distribution. It can also be seen that for the cooling air flow rate of 450 m^3/h a similar pattern is observed as in Figure 6.1 which is to be expected. Be that as it may, the case of 550 m^3/h shows an opposite trend compared to 450 m^3/h. This could be a seen as an error in the data, however this is unlikely to only show up here and as such this phenomena sofar remains unexplained.

Species concentrations Looking at the oxygen graph in Figure 6.6 a comparable trend in the curvature of the data lines is noticeable. All of the cases have an increased oxygen concentration near the burner nozzle where the combustion air is yet to react with the natural gas. The lines are ordered in sequence of lowest cooling air flow rate to the highest flow rate by having the lowest amount of

oxygen in the 360 m^3/h case up to the highest oxygen level in the 550 m^3/h case. Only the measured oxygen concentration for the 600 m^3/h cooling air flow rate case is lower than expected. Falling from 9 vol% as expected near the burner nozzle to as low as 5 vol% when the probe is not inserted in the furnace. Currently this difference cannot be explained, however it could be related to measurement inaccuracies but this remains to be seen in future experiments.
The NO graph for the Staggered 1 firing mode shows similar characteristics as for the parallel mode, see Figure 6.2. The 360 m^3/h curve shows the near burner zone perfectly with an emission of 10 ppm - 3% O_2 at a location of 10 cm from the nozzle. The absolute concentration is slightly lower compared to the parallel mode due to the higher temperature in the latter. Remarkable also are the "impossible" negative values for the lines of 550 m^3/h and 600 m^3/h. It is possible that the gas analyzer was not calibrated correctly, although the calibrating interval was never changed in any of the experiments. This could lead to a simple negative offset along the y-axis. This results in the same outcome as obtained for the parallel firing mode case, meaning hardly any NO was formed.

Figure 6.7 shows the CO_2 and CO graphs and it is clear to see that the CO data lines are quite different from those in the parallel firing mode. An almost perfect outline of the near burner zone was visible for the parallel case, but here the CO concentration is ever increasing with further insertion of the species probe. From theory it can be concluded that if high levels of CO are detected by the gas analyser, there has not been sample gas extraction directly from a near burner zone. Because of the changed flow pattern in the furnace due to the Staggered

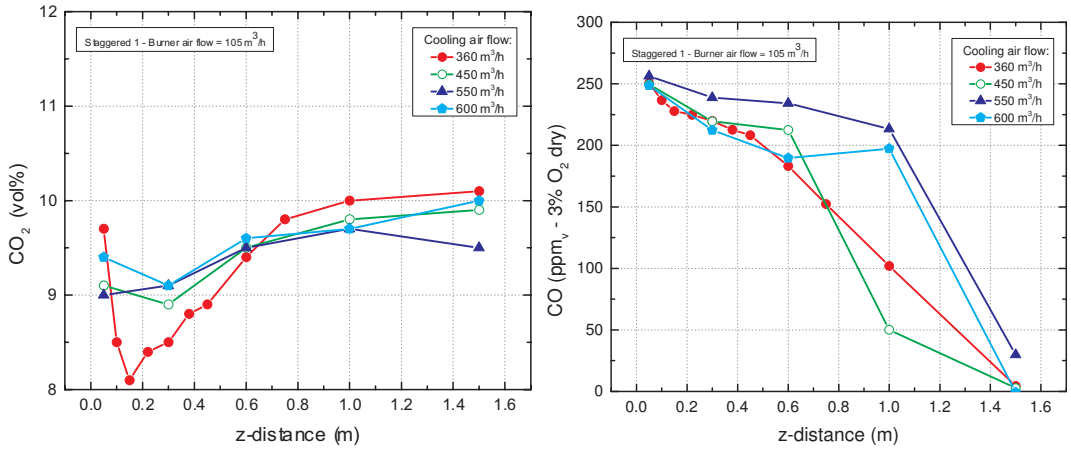

Figure 6.7: Staggered 1 firing mode. In the left graph the species concentration for CO_2 is displayed as a function of species probe insertion depth for several selected cooling air flow rates. On the right the CO concentration is shown for the same cases.

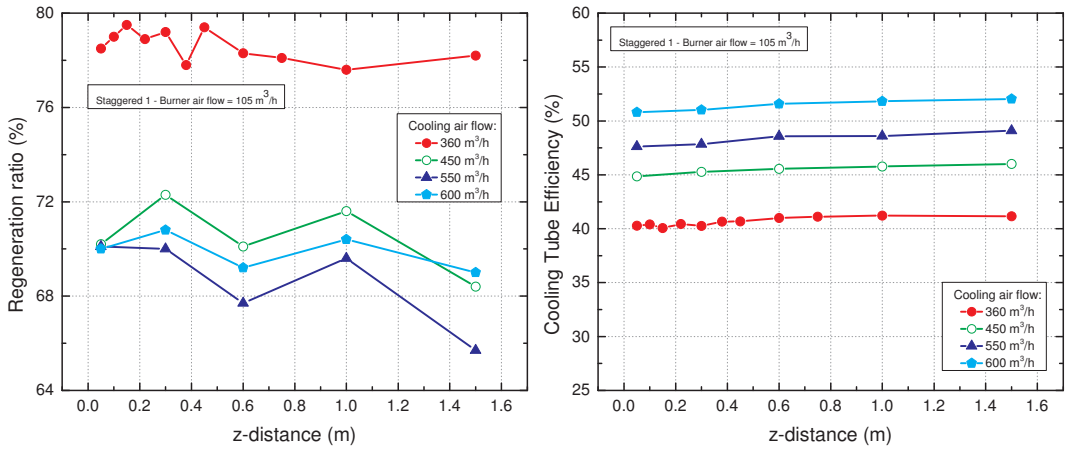

Figure 6.8: Staggered 1 firing mode. The regeneration rates (left) and cooling tube efficiencies (right) as a function of species probe insertion depth for varying cooling air flow rates are shown in this figure.

1 firing mode, CO could be sucked in from the firing burner at the same side effectively short-circuiting the flows, see Figure 4.2. This would, contrary to what was observed in parallel mode, result in a constantly higher CO concentration near the burner.
The CO_2 graph is basically the same as for the parallel case, except that the absolute values are slightly lower. This is due to a lower temperature and higher O_2 concentration for Staggered 1. This tells us that the reaction kinetics are slightly slower resulting in less optimal combustion.

Cooling Tube Efficiency and Regeneration ratio For the trends in the Cooling Tube Efficiency in Figure 6.8 the same explanation can be given as for the parallel firing mode. Higher cooling air flow rates correspond to higher CTEs which due to more heat that is extracted by the cooling tubes.
The regeneration lines are in the same range, percentage wise, as their parallel case counterparts, see Figure 6.4. The regeneration rate for the lowest cooling air rate, 360 m^3/h, is ($\approx 8-10\%$) higher than the other cases. This is something that was also seen before possibly indicating a direct or indirect relation between the cooling air rate and the regeneration percentage. this could be due to the way of measuring the flows (differential pressure) or perhaps it is due to a changing internal resistance for changing temperatures. Either way, the same effect is seen.

6.4 Burner air - Parallel

Temperature The temperature profiles for a varying amount of burner air flow rates can be seen in Figure 6.9. From the graphs of the furnace temperature the effect of the species probe insertion can easily be seen. The same effect as in the experiments for the changing cooling air flow rates occurred, resulting in significant temperature drops and thus affecting the steady state conditions in the furnace as well. The overall effect of the burner air flow rates on the furnace temperature manifests itself in a ΔT of $\pm 55°C$ going from 105 m^3/h to 125 m^3/h per burner. The data line for 125 m^3/h is higher than expected and falls between 105 and 110 m^3/h in terms of furnace temperature. The other cases are arranged by sequence according to the rule of lower burner air flow rates resulting in higher temperatures and vice versa.
The temperature uniformity is hardly affected as a function of burner air flow rate, as can be seen in Figure 6.9. This result was expected because the internal flow patterns do not change notably with changing flow rates. However from the same Figure it can also be seen that the temperature uniformity of the 125 m^3/h case is slightly higher, possibly indicating an increased mixing of the internal flue gases but it might also be related to the higher than expected furnace temperature. The difference is small nonetheless, which supports the statement of the temperature uniformity being *almost* constant with varying burner air flow rates.

Species concentrations Oxygen profiles show the near burner zone for all cases, see Figure 6.10. In fact this type of profile profile was previously seen in

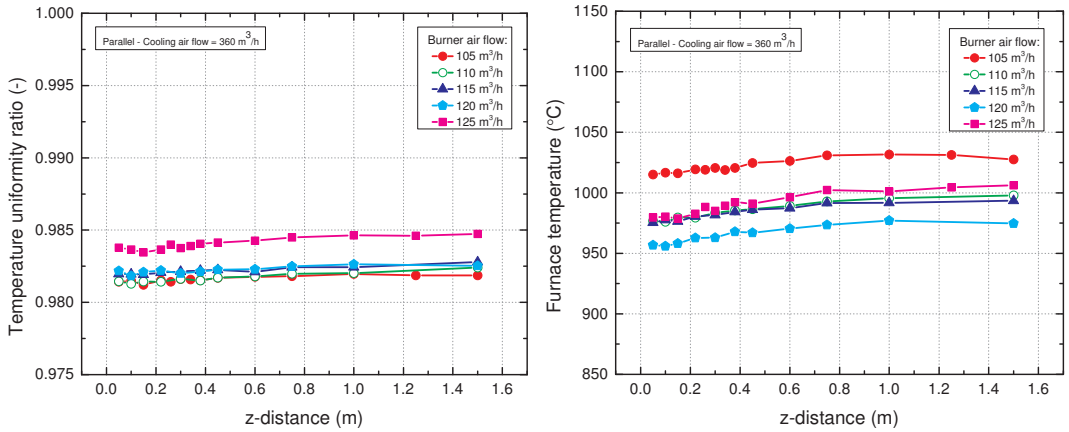

Figure 6.9: Parallel firing mode. In the left graph the temperature uniformity is shown as a function of the species probe insertion depth for several burner air flow rates. The furnace temperature is displayed on the right side for the same set of parameters.

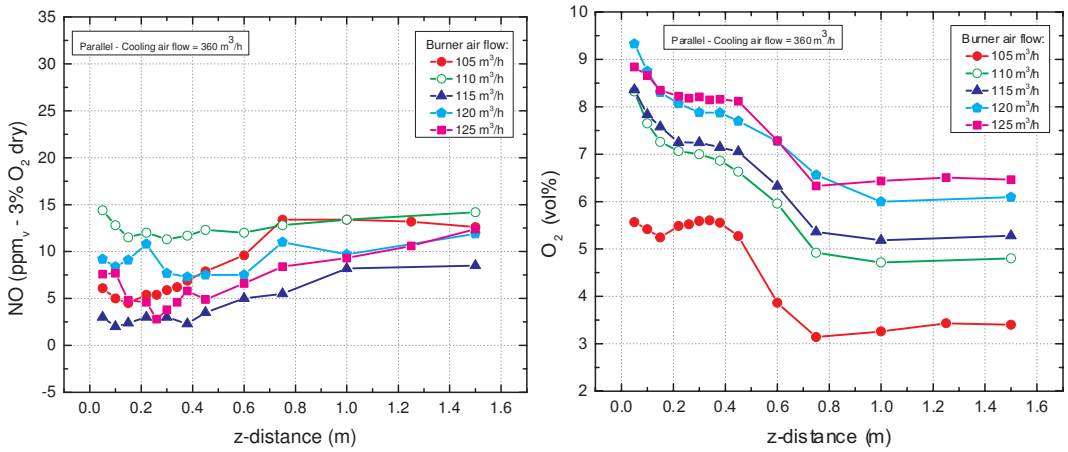

Figure 6.10: Parallel firing mode. On the left the NO species concentration is shown as a function of species probe insertion depth for several burner air flow rates. The oxygen concentration for the same cases is displayed on the right.

the parallel firing mode in Figure 6.2 for some of the lines. The lines for the 360 m^3/h cooling air flow rate and 105 m^3/h burner air flow rate are the same in both graphs because the data is from the same day, see Table 4.1. Having the similar profiles show up for all of the burner air flow rate cases begs the question why this did not happen for the varying cooling air flow rates. An explanation could be twofold; the temperature of the furnace affects the location and formation of the near burner zone greatly thus possibly resulting in it not being clearly visible for specifically low temperatures in the cases of varying cooling air flow rates.

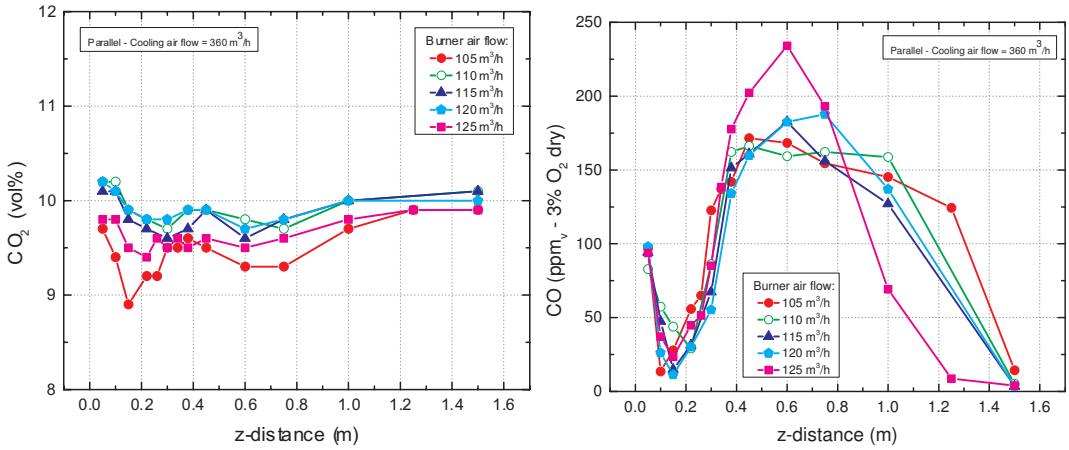

Figure 6.11: Parallel firing mode. The CO_2 species concentration profiles for the species probe insertion are displayed on the left for several burner air flow rates. The CO profiles are displayed on the right hand side of the figure for the same cases.

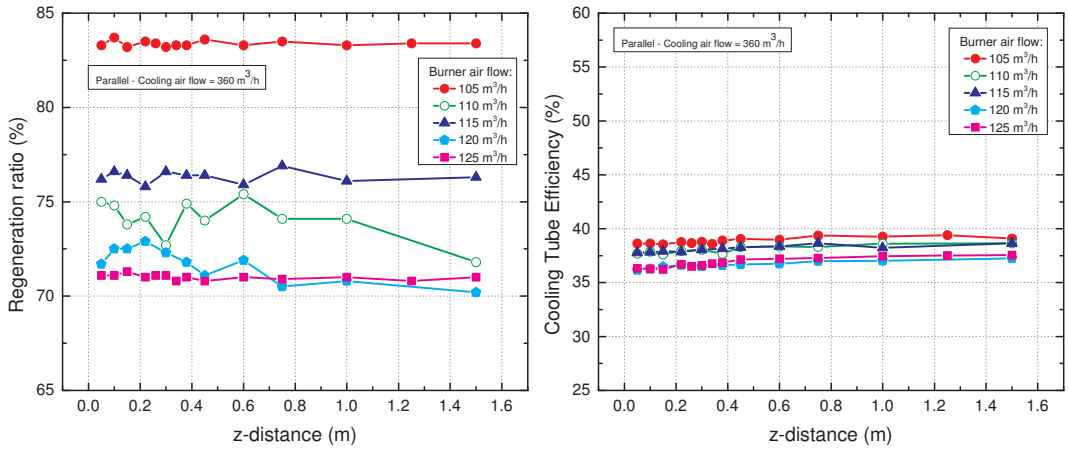

Figure 6.12: Parallel firing mode. The regeneration ratio expressed as percentage as a function of species probe insertion is displayed in the left graph for several burner air flow rates. The cooling tube efficiency is shown on the right for the same cases.

The other possibility is that the species probe is not able to collect reliable data for these specific cases and then as a result the similarity of the near burner zone profiles is not detectable in the graphs. Apart from these possible scenarios the data lines show nothing out of the ordinary. The oxygen concentration is highest for the highest burner air flow rate and lowest for the 105 m^3/h case.

Cooling Tube Efficiency and Regeneration ratio The regeneration percentage shows, just like in the previous cases, a much higher value for the lowest flow rate. This confirms the theory of lowest flow rates having a higher regeneration ratio. This might be due to either overall lower flow rates thus resulting in a higher value if the suction across the burners stay more or less constant. Or it might be due to the internal resistance for the air being lower for the flow over the heat exchanger than they are through the stack of the furnace.

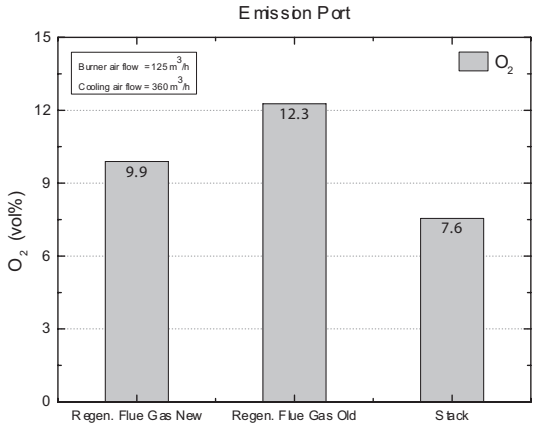

Figure 6.13: This figure shows averaged values of four cycles for three different measuring ports. Which data was used can be seen in Table 4.1.

6.5 Regenerative flue gas comparison

As explained in Chapter 3, new measuring points were created to find out what the impact of the flue gas recirculation and the induce fan on the oxygen concentration in the measured flue gases was. Figure 6.13 shows a difference of $\approx 2-3\%$ between the old and the new measuring point. This means that the value from the old point indeed is too high compared to the stack oxygen level. As a result, it can also be concluded that oxygen somehow enters the flue gas pipe in the vicinity of the induce fan, as shown in Figure 3.4.

6.6 CFD

The results from the CFD models, as described in Chapter 5, will be discussed in this section. Due to the nature of the simulations (steady-state) a direct comparison between the results from the species probe and the simulations will be difficult. The steady-state results in either having a flame at a specific burner or no flame at all while the experimental results are the outcome of a time averaged measurement, including both active and regenerative parts of the burner cycle.
NB: The results for data line *Case 2 - M - Flame* and *Case 2 - B - No flame* are inverted on the z-axis due to the burner being at the opposing wall in the staggered 1 firing mode. This a requirement because of the positioning of the burners in these cases and the definition of the z-axis that is used, see Figure 3.7. The names B - Flame , M - Flame refer to the burner location as determined in Table 5.1 being at the Bottom or Middle position.

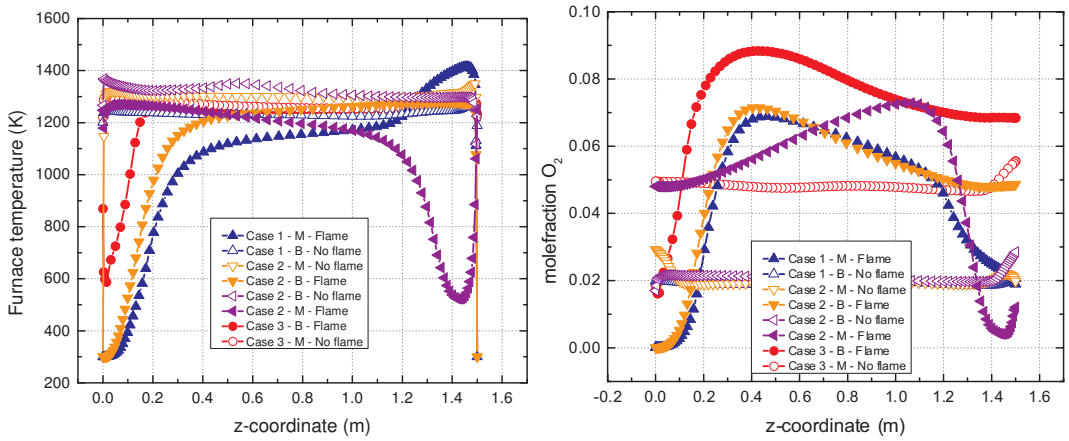

Figure 6.14: The furnace temperature is seen on the left for the three cases as described in Table 5.1. The right graph shows the oxygen mole fraction along the z-axis.

Temperature As seen in Figure 6.14 the furnace temperature for all of the cases are between 1200K and 1300K which coincides with the respective experimental cases. Unlike the measurements of global furnace temperature for the experimental results, the CFD shows an increase of the injected streams temperature from 300K up to the furnace temperature.
The furnace was not modelled with species probe; so the temperature effect is not present in the graph for the CFD models either. Thus the effect on local species concentrations because of the species probe presence is not taken into account either.

Species concentration The oxygen profile in Figure 6.14 shows a remarkable difference with the profile of the experiments because it starts with zero at the burner nozzle. This follows from the boundary conditions that are set for the CFD simulations but it also shows that the species probe extraction of flue gases already contains anywhere between 5-9% of oxygen depending on the specific case. This means that the burner air becomes mixed with the fuel and flue gases at a very short distance of the burner nozzle in reality. In the CFD data lines the oxygen mole fraction reaches a maximum further away from the nozzle to only then come down in the reaction zone.
From the same figure it can be seen that the lines for *Case 3 - B - Flame* and *Case 2 - B - Flame* are similar of shape ending with a relatively high oxygen concentration. These concentrations are normally only seen in the stack gases and indicate an under-estimation of the reaction rate.
The concentration profiles of CO_2 in Figure 6.15 have a different shape depending

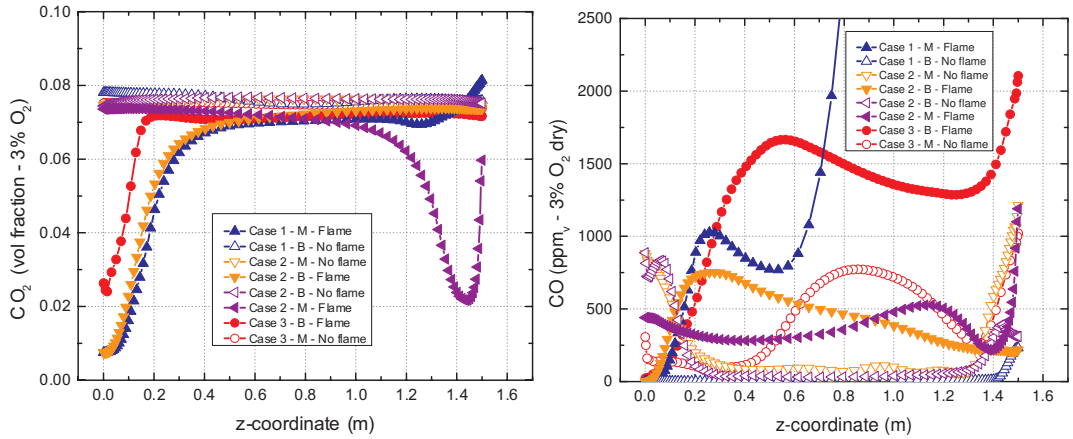

Figure 6.15: The CO_2 concentration can seen on the left for the three cases as described in Table 5.1. The right graph shows the CO concentration along the z-axis. This axis is the same as used for the experimental campaign so only the position of the flame changes depending on the presented curve.

on where the burners with flame are located. In two cases the flame is located on the bottom side and the other two flame locations are in the middle. The curves for the data lines is similar to the experimental results in the cases where no flame is present although $\approx 1-2\%$ lower. This could be due to the effect of incomplete combustion resulting in high CO, which can also be seen in the figure. For the cases with flame a new phenomena is displayed that could not be measured, due to averaging, and this is the CO_2 increase from the burner nozzle towards the furnace.

For the parallel cases (1 and 3) the curves show somewhat of the "hill" type shape except the scale is much larger. For the staggered case (2) the flame on the bottom shows a similar curve as in Figure 6.7. The line for the middle flame burner is inverted and does not show the same curve as clearly as for the parallel case resulting in a lower value at the regenerative side of the furnace. This is possibly because of the slight drop of the injection jet due to gravity pulling it down, as described by A. Jansen [1].

The species concentrations of NOx have been omitted in the overview of graphs because of unrealistically low emission predictions, as mentioned in the paper of E.S Cho et al. [2]. The concentrations are in the range of $0.35-0.70[ppm3\%O_2]$ which means hardly any NOx is produced and results in that NOx values of this order of magnitude cannot be used as a basis for conclusions. The NOx mechanisms are a post-processing step in the Ansys Fluent computational package and a such do not affect the CFD results discussed above.

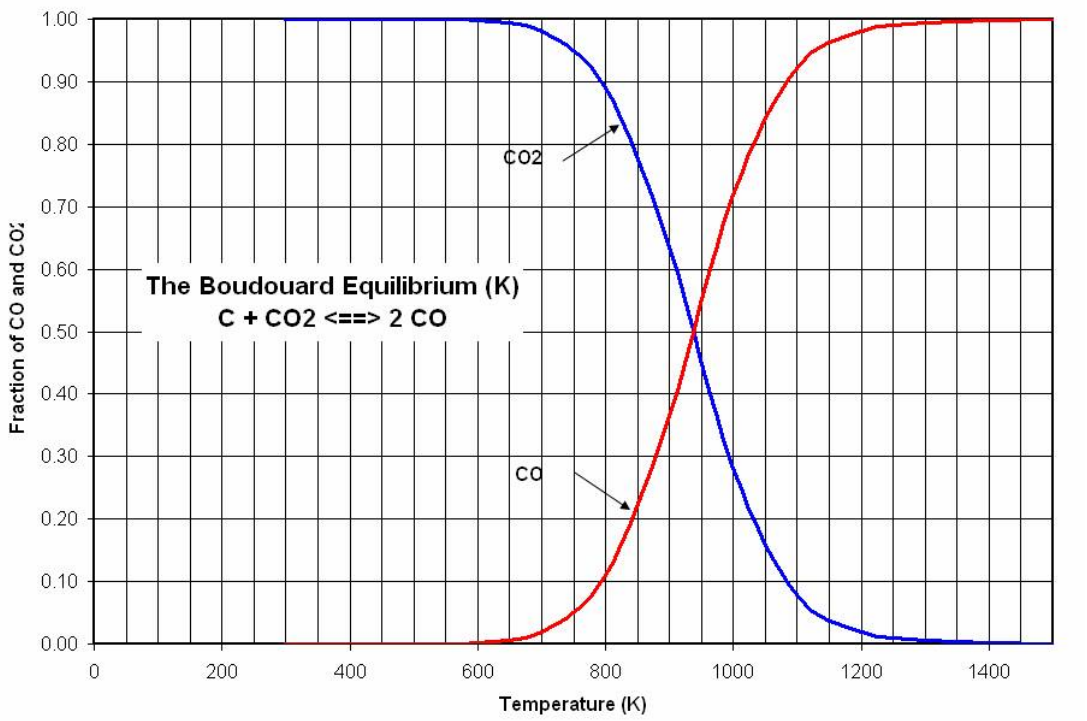

Figure 6.16: Graphical representation of the Boudouard equilibrium [3].

6.7 Species probe - Boudouard occurrence

Soot formation Introducing a water cooled probe into a furnace operating between $910°C$ and $1100°C$ turns out to be not as straightforward as it seems. Due to the probe being water cooled, the surface temperature of the probe will not exceed $80°C$ by design, assuming the furnace is operated at a capacity of $300kWh_{th}$. The surface temperature of the probe in the current ($200kWh_{th}$) state is expected to be lower.
Then in addition to the formation of combustion products a second type of reaction will take place when CO and CO_2 are both in the presence of a cold surface located within a hot furnace under atmospheric pressure. The result of this, soot, could visually be seen during the extraction of the probe as a deposit on the exterior surface of the probe. The layer of soot consisted of carbon, although samples have not been taken to determine the exact composition.
The formation of carbon deposits can be related to the following reaction, which is known as the Boudouard reaction.

$$2CO \rightleftharpoons CO_2 + C \tag{6.1}$$

Under normal conditions in the furnace, the balance between CO and CO_2 can be expressed shown as seen in Figure 6.16. From this figure it can be easily deducted that a rapid cool down of the gas in contact with the cold probe surface will result in the formation of carbon depositing on the cold surface of the probe. This possible occurrence of the reversed Boudouard reaction can influence the measurement by consuming part of the CO present in the air and converting it into CO_2 and so it has an effect on the measured local flue gas composition.
In fact the use of a cooled surface has been used in several other types of experiments [4] as a rather simple method of monitoring the deposition rate and subsequently the composition of the gases present in a furnace.

References

1. Jansen, A. *Numerical study on a multi-burner flameless oxidation furnace in relation to change in fuel composition.* Master's thesis, TU Delft (2012).
2. Cho, E. S., Shin, D., Lu, J., de Jong, W. & Roekaerts, D. Configuration effects of natural gas fired multi-pair regenerative burners in a flameless oxidation furnace on efficiency and emissions. *Applied Energy* **107**, 25–32 (2013).
3. Reed, T. Boudouard equilibrium. `http://gasifiers.bioenergylists.org/reedboudouard` (2006). [Online; accessed 27/02/2014].
4. Wang, G., Pinto, T. & Costa, M. Investigation on ash deposit formation during the co-firing of coal with agricultural residues in a large-scale laboratory furnace. *Fuel* **117, Part**, 269–277 (2014).

Chapter 7

Conclusions & Recommendations

7.1 Conclusions

Time-delay of measurement The measured transient delay of the system was determined to be less than 35s which means that there was sufficient settling time between switching of the sample gas extraction location and the moment data recording started. As a result, it is likely that the data is unaffected, or at least has a constant deviation, by the measuring delay.

Species probe The obtained species probe measurement results are very difficult to defend due to the severe in situ influence of the probe. Not only does it affect the global furnace temperature by $20 - 30°C$ but it can also lead to local disturbances on CO/CO_2 formation due to the Boudouard reaction. For now, it is not clear to what extend the Boudouard reaction has an effect on the measured sample gas, however, soot has been found on the outside of the species probe while extracting it from the furnace. As such, it is not recommended to be used as a validation tool for the current CFD model, which does not include a species probe.

Firing mode Comparing the results between Parallel and Staggered 1 firing mode, it can be concluded that parallel mode generally features the lowest emissions and a more uniform temperature distribution because of a better flow pattern inside the furnace.
Furthermore, the staggered 1 firing mode, as defined in Chapter 3, might be influenced by a short-circuiting of flows, Figure 4.2, directly from one firing burner into a regenerating burner. This can be defended by the high CO concentration values in the expected near burner zone as seen in Figure 6.7 caused by incomplete combustion or it could be because of the slight drop of the injected jet due to the significantly lower temperature, and higher density, of the injected stream compared to the furnace gases, resulting in a vertical drop in height of the stream as mentioned by A. Jansen.

CFD and species probe profiles The second part of the research objectives involved the wish to compare CFD simulation results with the species probe measurement data. After reviewing both results appears that they cannot be compared one-to-one due to the nature of the steady state simulations and the inherent unsteady state of the furnace in operation. This even goes so far that the author thinks the species probe measurements cannot be used as a basis for improving the currently existing CFD models due to the severe impact of the probe on the furnace conditions.

However, improvements can be made on the CFD model itself, possibly modelling a species probe to compare the experimental results under exactly the same furnace conditions.

7.2 Recommendations

Design of Experiments Although this thesis has barely scratched the surface of the possibilities of Design of Experiments, the author believes there is much to gain from further research. Especially the generation of designs from software packages is highly recommended in order to prevent unnecessary time-consuming experiments from being conducted. Making use of especially the split-plot design could prove a valuable addition to the research.

Calibration of gas analyzer As mentioned in Section 3.2 failure of regular calibration of the gas analyzer might result in the cross-interference for H_2O and CO_2. This issue can easily be resolved by a calibration once every year.

MEEC setup The experimental setup of the MEEC furnace can be improved in several ways. Namely, the gas analyzer should be replaced with another gas analyzer that can measure all the components at the same time, because the mechanical chopper is not the preferred type of device for continuous and fast measurements of all components. Progress is ongoing for selection of a new type of gas analyzer in order to achieve a better result and improve the accuracy of the measurement data.
For future experiments with simulated biofuels it is recommended to change the supply lines to the furnace as described in Section 3.4. This will require a static mixer to enable the DNG stream and dilution stream to be premixed before entering the flow line to the burners.

Appendix A

Data analysis

Analysis routine The MEEC furnace is equipped with a data acquisition system (DAQ) made by Beckhoff. This system can collect and store all connected sensors each second. The data is stored in ASCII text files which can easily be imported in the software of choice. Used here is the Tableau Business Intelligence software package which is freely available for students around the world. All the formulas required to form the heat and mass balances as well as the other parameters, as described by B. Danon and S. Darmawi, have been implemented into Tableau. As such, a large part of the formulas that are found in this Appendix are the same as described by the other authors. The main benefit of using a database-type of software package lies in the sometimes empty cells in the raw data file that are the result of errors coming from the DAQ system or connected sensors. It is these empty cells that makes analysis with more traditional software packages such as Matlab less desirable.
As said, the data is stored every second. Ten minutes was chosen for each data point. The starting six minutes of each connected data point acts as transient time to ensure a steady-state is reached. The data from the last four minutes is used for analysis. Thus, the average value over four full cycles is taken and displayed in Chapter 6. In the next couple of paragraphs, the exact data analysis routine will be described based on the formulas used. The reader is advised to read the Nomenclature at the beginning of this thesis for more information regarding the use of symbols in the following section.

Mass balance The fuel mass flow is determined via a volume flow measurement over a custom made orifice plate with a differential pressure sensor with the following equation:

$$\Phi^{\circ}_{v,fuel} = C_j \sqrt{\Delta p} \tag{A.1}$$

The molar mass of the supplied fuel is the weighted sum of all components in Dutch natural gas:

$$M_{fuel} = \sum_{i}^{N} M_i x_i \tag{A.2}$$

Based on the molar mass, the density can be calculated via the ideal gas law,

$$\rho^{\circ}_{fuel} = \frac{p^{\circ} M_{fuel}}{RT^{\circ}} \tag{A.3}$$

Lastly, the normal volume flow is converted to a mass flow:

$$\Phi_{m,fuel} = \Phi^{\circ}_{v,fuel} \rho^{\circ}_{fuel} \tag{A.4}$$

For the combustion air mass flow the volume flow is measured with a different set of differential pressure sensors. The actual recorded values are subsequently converted into a value under normal conditions using the ideal gas law with the following formula,

$$\Phi^{\circ}_{v,air} = \Phi_{v,air} \left(\frac{p_{air}}{p^{\circ}}\right) \left(\frac{T^{\circ}}{T_{air}}\right) \tag{A.5}$$

after which the mass flow ($\Phi_{m,air}$) can be determined by the same approach as Equation A.4.
Determination of the flue gas mass flow assumes complete combustion of one mole of fuel. The amount of moles of the main species are subsequently determined in the following equations:

$$n_{CO_2} = n_{fuel} \sum_{j}^{N} x_{j,fuel} \xi_{j,C} + n_{air} x_{CO_2,air} \tag{A.6}$$

$$n_{H_2O} = n_{fuel} \frac{1}{2} \sum_{j}^{N} x_{j,fuel} \xi_{j,H} \tag{A.7}$$

$$n_{O_2} = n_{fuel} x_{O_2,fuel} + (\lambda - 1)\, \gamma n_{fuel} x_{O_2,air} \tag{A.8}$$

$$n_{N_2} = n_{fuel} x_{N_2,fuel} + n_{air} x_{N_2,air} \tag{A.9}$$

The amount of excess air was could be calculated based on the measured value of oxygen in the sample gas.

$$\lambda = \frac{x_{O_2,air}}{x_{O_2,air} - [O_2]} \tag{A.10}$$

Then the normal volume flow and mass flow of the flue gas ($\Phi^{regen}_{m,flue}$) leaving the furnace via the regenerators was calculated based on the weighted molar mass of the flue gas.
After balancing the mass balance, the last term can be determined, which is the mass flow leaving the furnace via the stack ($\Phi^{stack}_{m,flue}$) resulting in the overall mass balance:

$$\frac{\partial m}{\partial t} = 0 = \Phi_{m,fuel} + \Phi_{m,air} - \left(\Phi^{regen}_{m,flue} + \Phi^{stack}_{m,flue}\right) \tag{A.11}$$

Heat balance The heat generated by the combustion of fuel consists of two components, the sensible heat and the chemical energy of the fuel.

$$Q_{fuel} = \Phi_{m,fuel} \left[\left(c_{p,fuel} T_{fuel,in} - c^{\circ}_{p,fuel} T^{\circ}\right) + \Delta H_{fuel}\right] \tag{A.12}$$

The specific heat of capacity of the fuel is determined by the molar weighted average of all the species multiplied by the heat capacity of each individual species:

$$c_{p,fuel} = \sum_{i}^{N} c_{p,i} x_i \tag{A.13}$$

For the combustion air heat flow the approach is similar as for the fuel except for the chemical energy, see equation.

$$Q_{air} = \Phi_{m,air} \left(c_{p,air} T_{air,in} - c^{\circ}_{p,air} T^{\circ} \right) \tag{A.14}$$

The heat capacity of air is taken as constant (1.293kJ/kg K) because of the small temperature variations for the incoming air.
The flue gas heat flow exiting the furnace is calculated with,

$$Q_{flue} = \left(\Phi^{regen}_{m,flue} + \Phi^{stack}_{m,flue} \right) \left(c_{p,flue} T_{flue} - c^{\circ}_{p,flue} T^{\circ} \right) \tag{A.15}$$

where the determination of the heat capacity is similar to the one discussed for the fuel.
The heat flow extracted from the cooling tubes is a function of the measured thermocouples in each of the tubes for the air coming in and going out as seen in Equation A.16.

$$Q_{cool} = \left(\Phi^{upper}_{m,cool} + \Phi^{lower}_{m,cool} \right) \left(c_{p,cool} T_{cool} - c_{p,air} T_{air} \right) \tag{A.16}$$

The heat extraction from the species probe (Q_{sp}) is assumed to be a linear function of insertion depth, more information can be found in Appendix D.
As a result, the heat losses from the furnace such as losses through the walls, cracks , environment and all other losses are the result of the total heat balance, as seen in Equation

$$\frac{\partial q}{\partial t} = 0 = Q_{fuel} + Q_{air} - Q_{flue} - Q_{cool} - Q_{sp} - Q_{loss} \tag{A.17}$$

Temperature uniformity The temperature uniformity is presented in the following equation,

$$T_u = 1 - \sqrt{\frac{1}{N} \sum_{i=1}^{N} \left(\frac{T_i - \bar{T}}{\bar{T}} \right)^2} \tag{A.18}$$

where N is the total number of temperature measurements positions in the furnace, T_i is the temperature in the i^{th} position and $\bar{T}$ is the mean of all the temperature measurements.
The value of T_u is between 0 and 1, where the value 1 indicates a perfectly uniform furnace.

Concentration correction In terms of species concentration a normalisation step is performed towards 3vol-% O_2 to be able to compare results, the calculation is as follows.

$$Concentration_{corrected} = Concentration_{measured} \left(\frac{21 - [O_2]_{reference}}{21 - [O_2]_{measured}} \right) \quad \text{(A.19)}$$

Cooling tube efficiency The cooling tube efficiency is an expression of the total amount of extracted heat by the upper and lower cooling tubes as a fraction of the total generated heat from the combustion reaction.

$$CTE = \frac{Q_{cool,out} - Q_{cool,in}}{Q_{fuel,in}} \quad \text{(A.20)}$$

Regeneration rate The regeneration rate is the mass of flue gas that leaves the furnace over the regenerator as a fraction of the total mass flow leaving the furnace.

$$\text{Regenerationratio} = \frac{\Phi^{regen}_{m,flue}}{\left(\Phi^{regen}_{m,flue} + \Phi^{stack}_{m,flue}\right)} 100\% \quad \text{(A.21)}$$

Appendix B

Heat up with Flame to Flox routine

Heat up Before experiments can be done in the MEEC furnace, the temperature inside of the furnace has to reach a steady-state. Due to the furnace being relatively large for a experimental setup it requires a relatively large time to heat up compared to small scale experimental setups. This results in more than a day required to heat up the furnace in an ideal situation. However, due to safety precautions in the facility it is not allowed to have the furnace active after 18:00, resulting in a forced cooling down to $700°C$ before letting it cool down further overnight. This sequence has to be repeated every day up till a stable steady-state temperature is reached, which is often not before Wednesday late during the day (assuming a start on Monday). This leaves very little time for experiments, so the maximum effective time for data collecting per week is around 8 - 10 hours when no problems arise.

Flame to Flox In the temperature range between $20°C$ and $\approx 860°C$ a regular flame is used for the supply of heat. Once the temperature has risen above this threshold, as measured by the furnace thermocouples, after a fixed amount of time the control systems of the furnace change the firing mode to FLOX. The result is a change in feed supply so that the air and fuel mix inside of the furnace instead of partially premix before entering the furnace, as seen in Figure B.1.

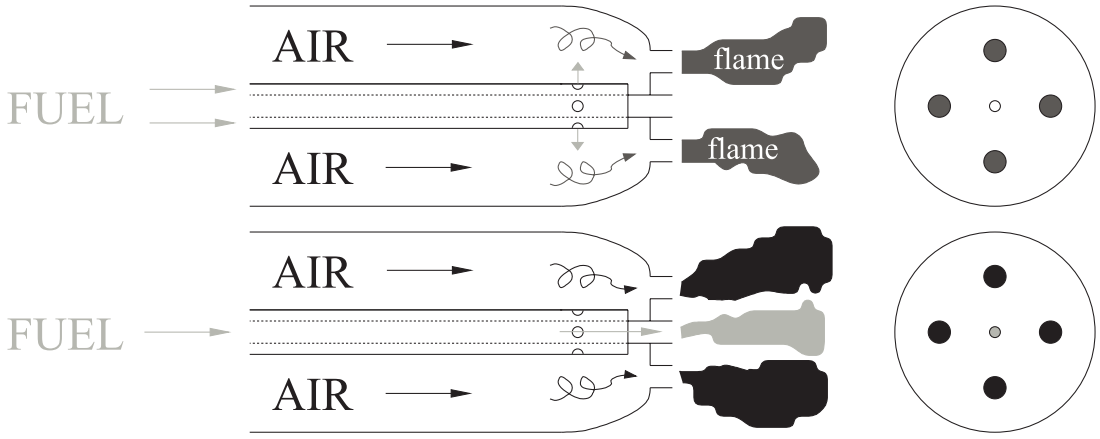

Figure B.1: In this figure the difference is shown between the flame (top) and the FLOX (bottom) firing modes. Picture made by B. Danon.

Appendix C

Near burner zone

Near burner zone The near burner zone in flameless combustion furnaces is the area where the injected streams come together with the entrained flue gases from inside the furnace. In this region, after mixing, the combustion reaction is initiated. Figure C.1 shows the reaction zone including the near burner zone.

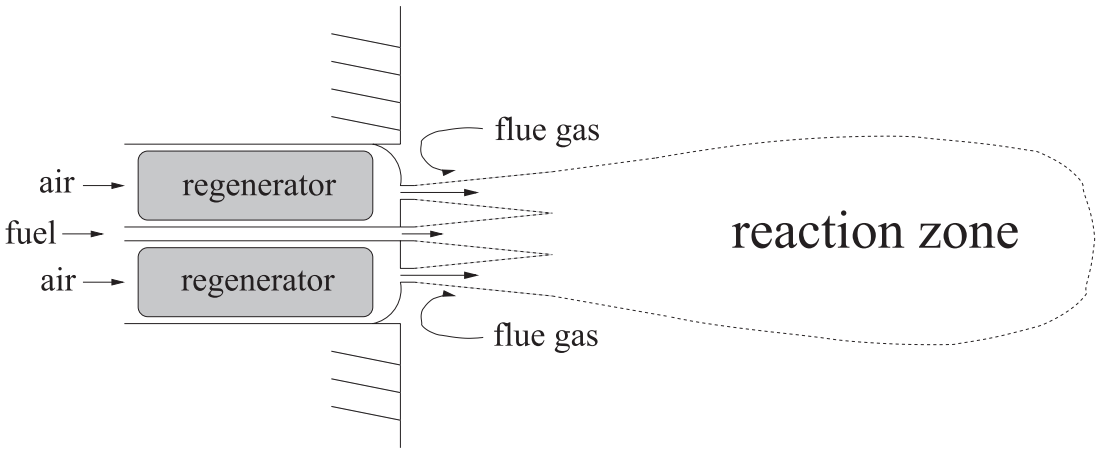

Figure C.1: In this figure the entrainment of flue gases can be seen which form the near burner zone when combustion initiates and subsequently flows over into the reaction zone. Picture made by B. Danon.

Appendix D

Species Probe heat extraction

Heat extraction Insertion of the species probe into the furnace results in the probe acting as a heat sink. With a mass flow specification of (30 - 40 l/min), which is constant for all experiments at 40 l/min, the assumption is made of constant ΔT ($= 10°C$) between the inlet and outlet of the probe as well. As a result, the heat extraction of the probe is a function of insertion depth which has a maximum cooling rate of $28kW_{th}$ when inserted close to the fuel nozzle resulting in a practical maximum cooling capacity of $\approx 27kW_{th}$ at the last species probe location of 5cm. The heat extraction of the species probe can be seen in Equation D.1.

$$\begin{aligned} Q_{\text{sp}} &= (\Phi_{\text{m,water}} \cdot c_{\text{p,water}} \cdot \Delta T) \left(\frac{z_{\text{inserted}}}{z_{\text{maximum}}}\right) \\ &= \left(1000 \cdot \left(40 \cdot 10^{-3}/60\right) \cdot 4200 \cdot 10\right) \left(\frac{z}{1.5}\right) \\ &= \approx 28 \left(\frac{z}{1.5}\right) [kW] \end{aligned} \tag{D.1}$$

The effect of these assumptions can best be seen in a heat balance graph for the losses. Such a graph can be seen in Figure D.1.

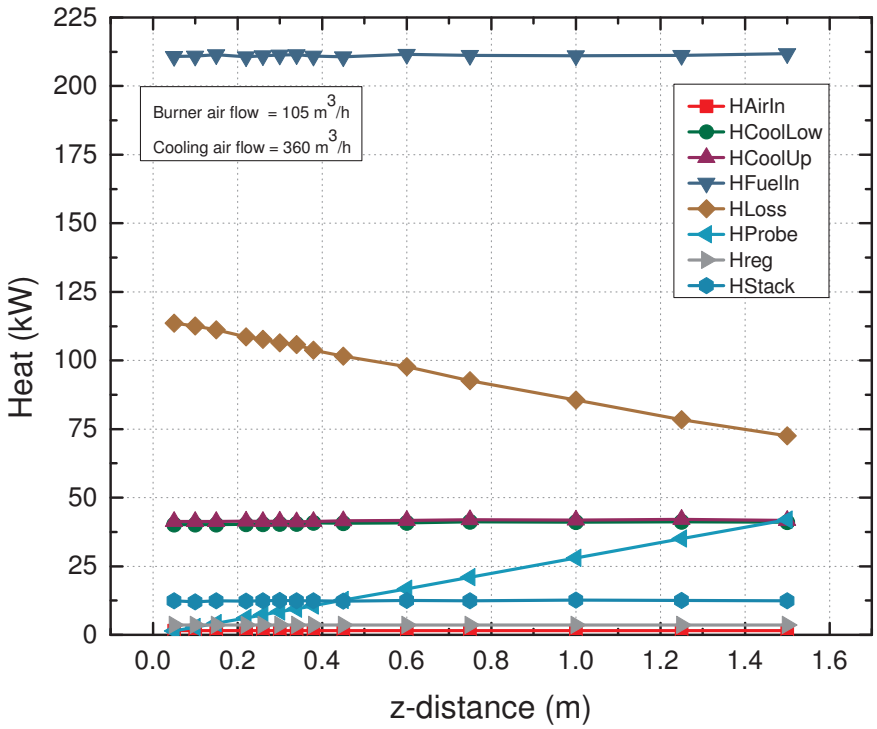

Figure D.1: This figure shows the heat input and outputs for the parallel firing mode with 360 m^3/h cooling air rate and 105 m^3/h burner air flow rate. The effect of the linear cooling capacity of the probe is clearly visible on both the HProbe and HLoss lines.